Real-time tracking of olfactory information, and correlating behavior with odor plume-encounters in an olfactory-guided navigation task: On why my ethanol plumes brought all the mice to the yard

Mohammad Farman Ul Haq Tariq

A dissertation

submitted in partial fulfillment

of the requirements for the degree of

Doctor of Philosophy

University of Washington

2023

Reading Committee:

David H. Gire, Chair

David J. Perkel, Co-chair

Sheri Mizumori

Jeffrey Riffell

Program Authorized to Offer Degree:

Neuroscience

University of Washington

Abstract

Real-time tracking of olfactory information, and correlating behavior with odor plume-encounters in an olfactory-guided navigation task: On why my ethanol plumes brought all the mice to the yard

Mohammad Farman Ul Haq Tariq

Chairs of Supervisory Committee:

David H. Gire

Department of Psychology

David J. Perkel

Departments of Biology & Otolaryngology

Understanding the neural underpinnings of sensory-guided decision-making has been one of the central pursuits of neuroscience. Olfaction is one key sensory modality that ensures the survival of a species by guiding essential behaviors like foraging, locating a mate, and shelter, and avoiding predation in individuals. Until recently, however, most of our understanding of the principles of mammalian olfactory neuroscience had been from studies using head-fixed preparations. How a complex olfactory stimulus in the form of a turbulent odor-plume guides navigation in mammals remains elusive. This lack-of-understanding stems from the challenges

associated with recreating the complex olfactory landscape that animals experience in the wild, and correlating the dynamic olfactory information with behavior and neural processing. Hence, in this thesis I summarize our approach in: 1) recreating the naturalistic behavior of plume-tracking in a lab using complex olfactory plumes, 2) using head-mounted sensors to record real-time olfactory and head-movement information during odor-guided navigation in mice, and 3) correlating behavioral adaptations with odor-plume contacts in freely moving mice engaged in an odor-guided navigation task.

Dedicated to Ammi Ji from whom, I am definite, I get all my resilience

Note

Chapter 1 of this thesis was published as a journal article in *eNeuro*, while Chapter 2 of this thesis will be submitted to a journal in future.

Acknowledgements

To my advisors David Gire and David Perkel: Thank you for being amazing advisors! Your mentorship has allowed me to grow as a scientist, stretching my skills to think critically, interpret results, and communicate those results to a wider audience. I did have some turbulent times during my graduate career, but you never lost the sight of my personal wellbeing by being patient with me when I needed patience and pushing me when I needed that extra push. I highly admire that both of you adapted your mentoring continuously based on what I needed, even if those needs were ever-changing much like my odor plumes ☺. I am so grateful for all the weekly discussions we have had, and the group-writing sessions before submitting the article.

To my committee members: Adrian KC Lee, Jeff Riffell, Sheri Mizumori, and **John Tuthill** you all provided me guidance on what more could be done, and I have appreciated your critical questions throughout the years.

To my mentors: Bill Walthall for taking me in your lab as an undergraduate, and for guiding me to a career in research. **Dabney Dixon** for shaping me to become a lively and interactive presenter. **Gennady Cymbalyuk,** and **Rob Clewley** for growing my computational skills. **Sarah Pallas** for making me ask the how and why questions when reading a research article in your course. **Jeff Smith, Hidehiko Koizumi, Naohiro Koshiya** and **Ruli Zhang** for introducing me to the field of respiratory neurobiology which made me appreciate central pattern generators, the main reason I joined neuroscience, even more.

To the members of the Gire and Perkel Labs: for your critical feedback before every major presentation.

To the undergraduate mentees: Aliena Lowell, and **Sidney Moore** for all those long days running mouse behavior in a dark and white noise-filled room. **Lane** for your computational skills to help me analyze the data.

To the friends I made in graduate school: Brian Jackson, Jesse Miles, Bryan Schuessler, and **Scott Sterrett** for making Guthrie Hall a fun place to work in, and especially to **Brian** for all those late-night remote-working sessions earlier in the pandemic that kept me productive. I cannot wait to spend more time with you in Germany.

To the Soft Bodies: Ryan Farero, Aaron Garcia, Michael Kiflezghi, David Qian, Raymond Sanchez, and **Rapheal Williams** for making graduate school fun. From spotting the Colonel Sanders lookalike, cracking jokes, freestyle Friday sessions, friendsgiving dinners, to being raucous and loud late into the night, I am extremely fortunate to share all these experiences and more with you all. Looking forward to the reunions in the future. **Michael,** and **Rapheal** special thanks for being my roommates for the last few years. **Aaron,** and **Ryan** for all those group projects during the first-year courses.

To my mom Shahida Naheed Riffat: Thank you for everything you have done for all of us. You have sacrificed a lot for us to prosper. I am extremely lucky to have you as my Ammi Ji.

To the rest of the Tariq family: although it is hard to deal with my siblings sometimes, I am fortunate to call you family, and thanks to my nephew and niece for allowing me to be the fun uncle.

Table of Contents

Introduction

Sensory processing, in head-fixed setups and involving learning paradigms, has been studied across a variety of behaviors for a range of mammalian species, including humans. While navigation has been studied for decades (Erdem et al., 2015; Gener et al., 2013; Herzog et al., 2019; Kolling et al., 2012), how it is accomplished using odors, and how periods of plume contact promote active sensation during navigation remain poorly explored (Marin et al., 2021). The olfactory system of mice is a well-suited model to study sensorimotor processing during the naturalistic behavior of plume-tracking due to the ethological importance of olfaction in rodents and the spatiotemporally complex olfactory information in the form of odor plumes. Studies using naturalistic behaviors in rodents (Dennis et al., 2021), in particular odor plume-guided navigation, have been historically limited due to the inability to experimentally monitor the complex odor plumes (Marin et al., 2021) that rodents encounter during free behavior. This thesis, hence, addresses two important gaps by presenting a method to record real-time olfactory information, and using that method to study how natural odor plumes shape active sensation of odor information during navigation, and the navigational strategy to spatially locate an odor source.

Odor delivery is governed by fluid dynamics

The spread of odor molecules emanating from a source is dependent on the physical laws governing the motion of the fluid. Currents of varying size and over different time scales exist in all fluids, be the fluid stationary or have a bulk flow. At the surface of contact between the source and fluid, fluid motion ceases, creating a layer of static fluid contact with the object. It is within this layer that diffusive forces, through Brownian motion of the molecules, are the predominant factors in creating a chemogradient.

However, this diffusive layer is very narrow, limiting the spread of molecules by diffusion to very short distances (<1 mm). Furthermore, spread via diffusion takes immensely long time to reach farther distances (Riffell et al., 2008). Above the very narrow diffusive layer, a velocity gradient, extending to 0.99 times the mean fluid velocity, exists within several layers. These layers, collectively, make up the boundary layer. The size of, and velocity profile within the boundary layer depends on the characteristics of the bulk flow and atmospheric conditions. Local directions of fluid velocity vary unpredictably within the boundary layer, creating spiraling pattern of eddies. These dynamically varying currents cause a turbulent mixing of the odor molecules with the fluid molecules. This mixture of odor and fluid molecules is additionally subjected to the bulk flow of the fluid.

The net result of these forces is a dynamically varying spread of the odor molecules in time and space as odor plumes (MURLIS J. and JONES C. D., 1981; Vickers, 2000; Webster D. R. and Weissburg M. J., 2001; Weissburg, 2000). Furthermore, the location of the source, in relation to the local topology, and active vs. passive release of the odor molecules also affect the shape of the odor plumes (Cardé and Willis, 2008; Vickers, 2000; Weissburg, 2000). Hence, time-averaged concentrations of the odorant in space is a poor measure of the odor profile that a non-stationary animal will experience.

Another key parameter, intermittency, the fraction of time an odor is detected at any one point, has to be considered to model the olfactory information available to the animal. Hence, limited studies have correlated behavior (Findley et al., 2021; Gire et al., 2016; Gumaste et al., 2020; Liu et al., 2020) with statistical features (Baker et al., 2018; Balkovsky and Shraiman, 2002; Celani et al., 2014; Celani and Seminara, 2005) present in the odor plume. However, these statistics

do not fully capture the plume's spatiotemporal variability that a moving animal will experience in real-time.

Strategies to localize chemical sources in freely behaving animals

The ability to navigate an environment using olfactory cues is one of the most evolutionarily conserved behavior and is exhibited by animals from different phyla. Animals engaged in odor tracking aid chemical detection with other senses, and display efficient strategies to localize the source of chemicals. In insects, navigation to chemical source has been shown to be achieved by anemotaxis (David and Kennedy, 1987; KENNEDY J. S., 1983; Kennedy John S., 1940; Kennedy and Marsh, 1974; Mafra-Neto and Cardé, 1998; Riffell et al., 2014; van Breugel and Dickinson, 2014; Vickers and Baker, 1994).

Upon sensing the odor molecules, they exhibit a *surging* behavior, in the upwind direction, that is maintained dependent on the contact with the molecules. If the contact is lost for an extended period of time, a crosswind *casting* behavior to re-establish contact with the odor plumes is initiated. Furthermore, this anemotactic behavior is modulated by the visual feedback during upwind motion (Kennedy John S., 1940; Wasserman et al., 2015).

Similarly, the upstream motion in crabs to localize chemical source has been shown to be guided by sensing the flow of fluid (rheotaxis) (Weissburg and Zimmer-Faust, 1993). In contrast, strategies used by mammals to localize airborne odors are not well understood. Recent studies have shown that mice might localize unfamiliar odor sources using concentration gradients (Findley et al., 2021; Gire et al., 2016). However, the plume generated in these studies allowed for frequent contact with the odor molecules.

Real-time recordings of the olfactory information using low-cost ethanol sensors

One of the challenges to correlate olfactory information with behavior had been the difficulty to quantify the odor molecules and precisely time the arrival of odor input to the animal during freely moving behaviors. Current technologies for chemical quantification are cumbersome and time-consuming. Chapter 1 of this thesis summarizes my research, performed in collaboration with other scientists within the Gire Lab, focused on implementing a method to allow for real-time quantification of the olfactory information that an animal receives.

We show the feasibility of using a modified low-cost ethanol sensor to achieve temporal and spatial sensitivity required to support real-time plume monitoring (Tariq et al., 2021). Furthermore, the lightweight of this sensor allows us to head-mount them on freely moving mice engaged in odor-guided navigation. Using this method, we show that plume encounters during navigation result in robust reduction in body speed. In addition, a separate line of research has established that the plume features detected by the sensors correlate with glomerular signals in the olfactory bulb of head-fixed mice (Lewis et al., 2021). Hence, this method allows an unprecedented quantitative analysis of behavior and the behavioral algorithm during plume-guided navigation.

Correlating mouse behavioral adaptations with plume-encounters during odor-guided navigation

Chapter 2 of this thesis builds on the work of Chapter 1 to combine real-time plume tracking with head-motions monitoring to study precise head-motion changes in response to olfactory information. A rich body of literature has shown that rodents actively increase their sniffing frequency and head orientation to maintain trail tracking (Jones and Urban, 2018; Khan et al., 2012; Rajan et al., 2006; Mathis et al., 2018). This increase in sniffing, correlated with head

movements (Karalis and Sirota, 2022; Liao and Kleinfeld, 2022), has also been recently suggested (Findley et al., 2021) to be involved in plume tracking during specific phases of gradient-difference dependent task. However, they were not able to establish the odor input-dependent changes in these head-motions.

Hence we show that mice show robust head-pitch motions in the 5-14Hz range, pointing to these motions as an active mechanism for sensory acquisition during plume-tracking. In addition, we show that these head-motions are increased right before plume encounters and are decreased in amplitude after encounters. We also show a reduction in body angles with respect to the source after encounters that is accompanied with a switch from rearing to foraging behavioral regime and increased frequency of head-motions.

References

Baker KL, Dickinson M, Findley TM, Gire DH, Louis M, Suver MP, Verhagen JV, Nagel KI, Smear MC (2018) Algorithms for Olfactory Search across Species. J Neurosci 38:9383.

Balkovsky E, Shraiman BI (2002) Olfactory search at high Reynolds number. Proc Natl Acad Sci 99:12589–12593.

Cardé RT, Willis MA (2008) Navigational Strategies Used by Insects to Find Distant, Wind-Borne Sources of Odor. J Chem Ecol 34:854–866.

Celani A, Seminara A (2005) Large-Scale Structure of Passive Scalar Turbulence. Phys Rev Lett 94:214503.

Celani A, Villermaux E, Vergassola M (2014) Odor Landscapes in Turbulent Environments. Phys Rev X 4:041015.

David CT, Kennedy JS (1987) The steering of zigzagging flight by male gypsy moths. Naturwissenschaften 74:194–196.

Dennis EJ, Hady AE, Michaiel A, Clemens A, Tervo DRG, Voigts J, Datta SR (2021) Systems Neuroscience of Natural Behaviors in Rodents. J Neurosci 41:911–919.

Erdem UM, Milford MJ, Hasselmo ME (2015) A hierarchical model of goal directed navigation selects trajectories in a visual environment. Neurobiol Learn Mem, Memory and decision making 117:109–121.

Findley TM, Wyrick DG, Cramer JL, Brown MA, Holcomb B, Attey R, Yeh D, Monasevitch E, Nouboussi N, Cullen I, Songco JO, King JF, Ahmadian Y, Smear MC (2021) Sniff-synchronized, gradient-guided olfactory search by freely moving mice. eLife 10:e58523.

Gener T, Perez-Mendez L, Sanchez-Vives MV (2013) Tactile modulation of hippocampal place fields. Hippocampus 23:1453–1462.

Gire DH, Kapoor V, Arrighi-Allisan A, Seminara A, Murthy VN (2016) Mice Develop Efficient Strategies for Foraging and Navigation Using Complex Natural Stimuli. Curr Biol 26:1261–1273.

Gumaste A, Coronas-Samano G, Hengenius J, Axman R, Connor EG, Baker KL, Ermentrout B, Crimaldi JP, Verhagen JV (2020) A Comparison between Mouse, *In Silico* , and Robot Odor Plume Navigation Reveals Advantages of Mouse Odor Tracking. eneuro 7:ENEURO.0212-19.2019.

Herzog LE, Pascual LM, Scott SJ, Mathieson ER, Katz DB, Jadhav SP (2019) Interaction of Taste and Place Coding in the Hippocampus. J Neurosci 39:3057–3069.

Jones PW, Urban NN (2018) Mice follow odor trails using stereo olfactory cues and rapid sniff to sniff comparisons. bioRxiv 293746.

Karalis N, Sirota A (2022) Breathing coordinates cortico-hippocampal dynamics in mice during offline states. Nat Commun 13:467.

KENNEDY J. S. (1983) Zigzagging and casting as a programmed response to wind-borne odour: a review. Physiol Entomol 8:109–120.

Kennedy John S. (1940) The Visual Responses of Flying Mosquitoes. Proc Zool Soc Lond A109:221–242.

Kennedy JS, Marsh D (1974) Pheromone-Regulated Anemotaxis in Flying Moths. Science 184:999.

Khan AG, Sarangi M, Bhalla US (2012) Rats track odour trails accurately using a multi-layered strategy with near-optimal sampling. Nat Commun 3:703.

Kolling N, Behrens TEJ, Mars RB, Rushworth MFS (2012) Neural Mechanisms of Foraging. Science 336:95–98.

Lewis SM, Xu L, Rigolli N, Tariq MF, Stern M, Seminara A, Gire DH (2021) Plume dynamics structure the spatiotemporal activity of glomerular networks in the mouse olfactory bulb. Front Cell Neurosci 15.

Liao S-M, Kleinfeld D (2022) A change in behavioral state switches the pattern of motor output that underlies rhythmic head and orofacial movements (preprint). Neuroscience.

Liu A, Papale AE, Hengenius J, Patel K, Ermentrout B, Urban NN (2020) Mouse Navigation Strategies for Odor Source Localization. Front Neurosci 14:218.

Mafra-Neto A, Cardé RT (1998) Rate of realized interception of pheromone pulses in different wind speeds modulates almond moth orientation. J Comp Physiol A 182:563–572.

Marin AC, Schaefer AT, Ackels T (2021) Spatial information from the odour environment in mammalian olfaction. Cell Tissue Res 383:473–483.

Mathis A, Mamidanna P, Cury KM, Abe T, Murthy VN, Mathis MW, Bethge M (2018) DeepLabCut: markerless pose estimation of user-defined body parts with deep learning. Nat Neurosci 21:1281–1289.

MURLIS J., JONES C. D. (1981) Fine-scale structure of odour plumes in relation to insect orientation to distant pheromone and other attractant sources. Physiol Entomol 6:71–86.

Rajan R, Clement JP, Bhalla US (2006) Rats Smell in Stereo. Science 311:666.

Riffell JA, Abrell L, Hildebrand JG (2008) Physical Processes and Real-Time Chemical Measurement of the Insect Olfactory Environment. J Chem Ecol 34:837–853.

Riffell JA, Shlizerman E, Sanders E, Abrell L, Medina B, Hinterwirth AJ, Kutz JN (2014) Flower discrimination by pollinators in a dynamic chemical environment. Science 344:1515.

Tariq MF, Lewis SM, Lowell A, Moore S, Miles JT, Perkel DJ, Gire DH (2021) Using Head-Mounted Ethanol Sensors to Monitor Olfactory Information and Determine Behavioral

Changes Associated with Ethanol-Plume Contact during Mouse Odor-Guided Navigation. eNeuro 8.

van Breugel F, Dickinson MH (2014) Plume-Tracking Behavior of Flying Drosophila Emerges from a Set of Distinct Sensory-Motor Reflexes. Curr Biol 24:274–286.

Vickers N (2000) Mechanisms of animal navigation in odor plumes. Biol Bull 198:203–212.

Vickers NJ, Baker TC (1994) Reiterative responses to single strands of odor promote sustained upwind flight and odor source location by moths. Proc Natl Acad Sci 91:5756.

Wasserman SM, Aptekar JW, Lu P, Nguyen J, Wang AL, Keles MF, Grygoruk A, Krantz DE, Larsen C, Frye MA (2015) Olfactory Neuromodulation of Motion Vision Circuitry in Drosophila. Curr Biol 25:467–472.

Webster D. R., Weissburg M. J. (2001) Chemosensory guidance cues in a turbulent chemical odor plume. Limnol Oceanogr 46:1034–1047.

Weissburg M (2000) The fluid dynamical context of chemosensory behavior. Biol Bull 198:188–202.

Weissburg MJ, Zimmer-Faust RK (1993) Life and Death in Moving Fluids: Hydrodynamic Effects on Chemosensory-Mediated Predation. Ecology 74:1428–1443.

Using head-mounted ethanol sensors to monitor olfactory information and determine behavioral changes associated with ethanol-plume contact during mouse odor-guided navigation

Mohammad F. Tariq[1,2,4], Suzanne M. Lewis[2], Aliena Lowell[2], Sidney Moore[2], Jesse T. Miles[1,2], David J. Perkel[3,4], David H. Gire[2,4]

[1]Graduate Program in Neuroscience, [2]Department of Psychology, [3]Departments of Biology & Otolaryngology, University of Washington, [4]University of Washington Institute for Neuroengineering

Abstract

Olfaction guides navigation and decision-making in organisms from multiple animal phyla. Understanding how animals use olfactory cues to guide navigation is a complicated problem for two main reasons. First, the sensory cues used to guide animals to the source of an odor consist of volatile molecules, which form plumes. These plumes are governed by turbulent air currents, resulting in an intermittent and spatiotemporally varying olfactory signal. A second problem is that the technologies for chemical quantification are cumbersome and cannot be used to detect what the freely-moving animal senses in real time. Understanding how the olfactory system guides this behavior requires knowing the sensory cues and the accompanying brain signals during navigation. Here we present a method for real-time monitoring of olfactory information using low-cost, lightweight sensors that robustly detect common solvent molecules, like alcohols, and can be easily mounted on the heads of freely behaving mice engaged in odor-guided navigation. To establish the accuracy and temporal response properties of these sensors we compared their responses with those of a photoionization detector (PID) to precisely controlled ethanol stimuli. Ethanol sensor recordings, deconvolved using a difference-of-exponentials kernel, showed robust correlations

with the PID signal at behaviorally relevant time, frequency and spatial scales. Additionally, calcium imaging of odor responses from the olfactory bulbs of awake, head-fixed mice showed strong correlations with ethanol plume contacts detected by these sensors. Finally, freely behaving mice engaged in odor-guided navigation showed robust behavioral changes such as speed reduction that corresponded to ethanol plume contacts.

Significance Statement

Animals are remarkable at locating resources, essential to survival, from long distances using olfactory information. Understanding the neurophysiological mechanisms and the behavioral strategies for accomplishing this goal has been challenging due to the intermittent nature of the olfactory information. Here we present a method to record real-time olfactory information using low cost, lightweight sensors that can be mounted on the head of freely behaving rodents. This technology can therefore allow us to better correlate the spatiotemporally varying intermittent olfactory information with behavioral changes and neurophysiological recordings.

Introduction

Animals from different phyla within the kingdom use olfactory cues to guide navigation and decision-making to find resources essential to survival. This task of locating resources using olfaction is a complex problem due to the nature of the olfactory stimulus. Odor molecules emanating from a source spread due to turbulent air currents (Celani et al., 2014; Celani and Seminara, 2005). These dynamically varying currents result in stochastic mixing of the odor molecules with the fluid molecules. The net result of these turbulent forces is a dynamically varying spread of odor molecules in time and space as odor plumes. Hence, time-averaged concentrations of the odorant in space are a poor measure of the olfactory information that a freely moving searcher, using odors to find the source, will experience (Baker et al., 2018). Measuring this odor input in real-time, as sensed by the searcher, is essential to understanding how the nervous system processes olfactory information during complex free behavior such as plume tracking.

Current technologies for chemical quantification are not feasible for mobile operations. Photoionization detection (PID) is a technology that is routinely used by olfactory researchers (Riffell et al., 2008), but the sensor in this case is also relatively large and expensive. A technology used to study odor-guided navigation by insects is electroantennography (EAG) (Justus et al., 2005). EAG sensors are small, lightweight and highly sensitive to volatile compounds. However, EAG signals are also highly sensitive to changes in air pressure and temperature, and often degrade over the time scale of hours, which precludes the use of the same EAG sensor on multiple animals. We thus employed a method for using lightweight and low-cost metal oxide gas sensors that are used in environmental chemical detection systems (Wang et al., 2010) as a feasible method for relatively rapid mobile monitoring of the odor environment.

One limitation of using the metal oxide sensors is the long decay time of the sensor recordings in response to transient activation with the chemical stimulus. Here we first conducted paired alcohol-sensor and PID recordings to pulsed and naturally fluctuating ethanol stimuli and developed a method to deconvolve the sensor recordings to improve the response time and increase the match with PID recordings. This deconvolution methods is similar to approaches that have been successfully used in robotics contexts (Martinez et al., 2019), and produces similar results. Furthermore, we present results correlating the deconvolved alcohol-sensor signals to calcium imaging responses in head-fixed mice. Additionally, results from freely navigating mice engaged in localizing an ethanol odor-source show speed reductions upon ethanol plume contacts detected by the head-mounted alcohol sensors. This method can serve as a cost-effective way to correlate real-time olfactory information with behavior and physiological responses during olfactory navigation tasks.

Materials and Methods

The designs for the 3D printed parts and software used to analyze the alcohol sensor recordings will be publicly available at the author's website upon publication.

Paired PID and ethanol sensor recordings

Figaro TGS 2620 Organic Solvent Vapor Sensor (powered by a 5V DC voltage from an Arduino [Adafruit]) was used to monitor the relative concentration of ethanol vapors in the air. To prevent extended contact of odor-laced air with the sensor, the head cap of the sensor was removed. Paired PID and alcohol sensor recordings were then conducted ~10-15 mm downstream of an odor port releasing ethanol vapors from a tube controlled by a valve (Clippard EV-2-12). The PID and sensor recordings were digitized by NI USB-6009 DAQ (National Instruments) at a sampling

frequency of 500 Hz. The data acquisition and valve control were carried out through custom scripts written in LabView (National Instruments). For recordings in a dynamic plume, paired recordings were carried out downwind of an ethanol port in a custom-designed arena (see below) at multiple locations. Data from locations near the port, near the middle of the arena, and farthest downwind were pooled.

Deconvolution of the ethanol sensor signal

The raw alcohol sensor recordings were low-pass filtered using a digital filter in MATLAB (Mathworks) (cutoff frequency: 40 Hz). The frequency content in the filtered signal was then obtained by the *fft* routine. A difference-of-two-exponentials kernel (Monroy et al., 2012) was then designed (see Results) using the equation:

$$f(t) = \exp\left(-\frac{t}{\tau_{Decay}}\right) - \exp\left(-\frac{t}{\tau_{Rise}}\right)$$

The frequency content of the kernel, obtained by the *fft* routine, was then used to divide the filtered signal. The resulting spectrum was then converted back into the time domain by taking the *ifft* of the signal. The difference between the PID recording and the deconvolved signal was calculated by normalizing both signals to their maximum values. This allowed for the comparison of the waveform of the two signals with no particular emphasis on the amplitude of the responses. Values for τ_{Rise} of 2 ms and τ_{Decay} of 0.5 s minimized the least-squares error between the deconvolved sensor and the PID signals.

Animal care

All animal procedures were performed in accordance with the [Author University] institutional animal care committee's regulations. All mice strains were obtained from JAX laboratory and maintained in local colonies with ad libitum food supply. After surgical procedures, each animal was singly housed. The colony was maintained on reverse 12 hrs light schedule (7AM

lights off; 7PM lights on) with behavioral experiments performed during the dark cycle (Zeitgeber times: ZT12-23).

Calcium signals from the OB of awake animals

For calcium imaging of active glomeruli in response to alcohol plumes, an imaging window was placed over the dorsal main olfactory bulb (OB) of Thy1-GCaMP6f-GP5.11 (Dana et al., 2014) mice using methods, described previously (Batista-Brito et al., 2017). Following recovery from the surgery, imaging sessions were conducted while each mouse was head-fixed under a widefield microscope within a wind tunnel during alcohol plume presentations. In the wind tunnel the odor was carried downwind from an odor port located 13.5 cm from the nose of the head-fixed animal. To record ethanol signals, an alcohol sensor was placed within 4mm of the right nostril. The calcium signals were then spatially segmented using CNMF (Pnevmatikakis et al., 2016), and the alcohol sensor recordings deconvolved (see above). In the wind tunnel odors were transported as turbulent plumes, making the time of arrival variable from trial to trial. The calcium responses from each glomerulus were therefore aligned with respect to the first peak recorded by the ethanol sensor for each trial to study the ethanol-evoked responses within the projection neurons of the OB.

Behavioral apparatus

The arena to study plume tracking in freely moving animals was constructed as reported previously (Jackson et al., 2020). Briefly, the arena (2m (l), 0.9m (w), 0.9 m (h)) was constructed using aluminum railings and closed off using clear acrylic along the length. Furthermore, a clear acrylic sheet was placed on top to close off the air supply. The floor was a sheet of opaque white acrylic. The two smaller ends were covered by a thin film of mesh to allow air currents to pass in a directional manner. Furthermore, an exhaust fan spanning the width of one half of one end of the

arena created a directional air movement pattern (see Figs. 5A, 7C & 7D). The nesting area was placed outside the arena and constructed from clear acrylic, with a small passage into the arena gated by a motor under LabView control. A custom designed mechanism, under Arduino control, was used to position the odor port (5-10 mm distance from the arena floor) at any x-y location within the arena. The odor stimulus consisted of passing air, controlled by valves (Clippard EV-2-12), from a tube filled with pure ethanol, resulting in ethanol vapor introduced via a clear plastic tube through the odor port into the arena. Colocalized with the odor port was the port to deliver reward (water droplets), which was also controlled with valves. An overhead camera (Basler acA640-90uc; Frame Rate: 90fps) was used to record the behavior and the position of the odor and reward ports within the arena.

Simultaneous behavioral and olfactory information tracking from freely moving mice

Five WT littermates mice (5 months old at implantation; 2 males/3 females; strain no: 024105 JAX lab; C57BL/6J background) were used as subjects. Each mouse underwent aseptic surgery, with isoflurane as anesthetic, to affix a 3D printed sensor mount, which housed 4 magnets (K&J Magnetics D101-N52), to the skull. Separately, the sensor was affixed to a second 3D printed part, which contained 4 magnets in opposite polarity to the head-mounted part. This part could nest inside the head-mounted part. This configuration allowed rapid placement and removal of the sensor on the animal's head. After surgery, each mouse was housed singly.

Following a rest period (>2 weeks) to recover from surgery, mice were water deprived and trained to associate water reward with the ethanol odor. This training was achieved by placing a weigh boat, containing water reward with an ethanol-soaked pad taped to the bottom, in the home cage for at least 15 mins. The training lasted for >1 week and was carried out during the dark phase (ZT12-23). Each mouse was then maintained at >85% of the pre-deprivation body weight. After 1

week of association, animals were acclimatized to handling and restraining by the experimenters during 5-10 minute sessions for each mouse. Each mouse then underwent further sessions while wearing a head-mounted sensor in its respective cage. Following the association and acclimatization with the sensor, each mouse was then introduced into the arena for exploration in 15 minute sessions over the course of 3 days. The association was carried out in a different room than the room housing the arena.

To remove visual and auditory cues during the odor-source localization task within the behavioral arena, all the trials were conducted under infrared illumination, and with white noise played continuously on the speakers. Each trial started by first placing the odor port at one of the six chosen locations within the arena and turning on the odor stimulus. The gate from the nesting area was then opened and the mouse allowed to enter the arena. Once the mouse entered the arena, the gate to the housing cage was closed and the mouse was allowed to navigate to the location of the odor port to receive the reward. For the initial few trials, water droplets were dropped onto the floor of the arena until the animal improved in localizing the odor port. The order of the location of the odor port and the animal testing order was randomized each day.

Once the animal navigated to the odor port and received the water reward, a 1-kHz tone played for 1s, signifying the end of trial and the gate to the nesting area opened. During the period from the end of the trial and the return of the animal to the nesting arena, the odor stimulus was turned off. For trials where the mouse took longer than approximately 5 mins to return to the arena, the mouse was gently coaxed back into the nesting area by an experimenter. Each mouse completed 4-12 trials each day. Once each animal was proficient in localizing the odor port, assessed qualitatively, trials with the head-mounted sensors were conducted in the behavioral arena. The data presented here are only from the trials when the sensor was mounted during the behavior.

Analysis of the real-time olfactory information and behavior from freely behaving mice

All analysis software was written in MATLAB 2019a. The videos were analyzed by foreground and background separation using Dynamic Mode Decomposition (Grosek and Kutz, 2014). The body was discernible due to the dark fur against white background, while the head position was obtained using an LED mounted on the sensor body during the behavior. The resulting pixel cloud was then used to estimate the center of mass, allowing determination of the body and head positions. These position coordinates were further low-pass filtered to remove jitter. Speed was calculated as the distance traveled between each successive frame. The alcohol sensor recording was deconvolved as outlined above, but the τ_{Rise} constant was adjusted to 20 ms and the τ_{Decay} constant was adjusted to 2.0 s to minimize spurious detection of small signals due to head movement. The trajectories and sensor recordings for each trial were analyzed only between when the animal entered the arena and when it received the reward. User-defined thresholds for event crossings, detected by Schmitt Trigger (Mathworks File Exchange), were then set for the deconvolved signal from each trial. The deconvolved signal was further normalized by calculating the fractional deviation from the average baseline signal (mean of the signal during the initial 1s upon entry of the animal into the arena) as dx/x. Only event crossings separated by greater than 5s were considered as separate plume encounters. Furthermore, the animal had to be further than 10 pixels from the odor source at the time of the event crossing. 177 contacts from 88 trials passed these criteria. The body and head speeds, and the normalized deconvolved alcohol signal was then obtained in a 4s window surrounding plume contacts, and these signals were averaged to obtain the mean time course. As control, equal time-sized portions of trajectories that did not contain plume contact were randomly selected.

Results

Difference of two exponentials kernel to deconvolve the raw alcohol sensor responses

We first tested the feasibility of the ethanol sensor to record behaviorally relevant odor stimuli by conducting paired PID and ethanol-sensor recordings in response to brief ethanol stimuli (Fig. 1A). As can be seen, the ethanol sensor recordings decay more slowly than the PID responses. To improve our understanding of the rise time and decay time of the ethanol sensor responses, the individual recordings were averaged to determine the mean time rise and tau decay. The mean rise and decay signals (Fig. 1B) were then exponentially fit to obtain the τ_{Rise} (0.06 s) and τ_{Decay} (3.5 s). Modeling the ethanol response as a difference of two exponentials (Monroy et al., 2012), we deconvolved individual ethanol-sensor recordings using a family of kernels with a range of tau rise and tau decay values. These deconvolved signals were then compared with the PID recordings, taken as the ground truth. The dependence of the mean error between the deconvolved sensor recordings and the PID recordings as a function of tau rise and tau decay values of the kernel is presented in Fig. 1C. Based on this information, we set the value of τ_{Rise} for the kernel to be 2 ms and that of τ_{Decay} to be 0.5 s. Using this kernel, the raw ethanol recordings presented in Fig. 1A were deconvolved and are shown in Fig. 1D. For comparison, the PID response is shown in red. The inset shows the normalized PID and deconvolved response to better compare the waveform of the two sensors. To test whether a major shift occurred due to the deconvolution procedure, we compared the threshold-crossing times (time to 5% of the max from the valve opening) of the deconvolved signal and the PID responses (Fig. 1E) for individual ethanol presentations. A linear relation ($r = 0.9391$, $p<0.001$) exists between the threshold-crossing time of the deconvolved signal and the PID responses. This linear relationship decreased if only data presented in the inset of Fig 1E are used to compute the correlations ($r = 0.1991$, $p = 0.0139$). This decrease in correlation could

be due to the different dynamic ranges, and active vs. passive nature of the PID and the alcohol sensor (see Discussion).

The summary data from brief pulses (0.3 s and less) are presented in Fig. 2A as a heatmap where each row represents a single trial aligned with respect to the valve opening. The PID responses are presented in red, while the deconvolved ethanol sensor signals are presented in blue. Overlaying the two responses we can see coincident activity in magenta (right). Furthermore, the peak times (time of the maximum amplitude response with respect to the valve opening) of the deconvolved signal and the PID response (Fig. 2B) show a linear relationship ($r = 0.8903$, $p < 0.001$) indicating the coincident activity of the two sensors. Deconvolution of the ethanol-sensor signal thus provides an adequate approximation of the real-time odor concentration.

Frequency characteristics of the ethanol sensor

We then tested the range of frequencies at which the ethanol sensor can detect signals by conducting paired PID and alcohol-sensor recordings to ethanol pulse stimuli of 5, 10 and 15 Hz frequencies. Fig. 3A shows the raw ethanol sensor and PID recordings for single trials of the frequencies tested. The raw sensor recordings were then deconvolved using the same kernel as used for the single pulses (see above). The deconvolved signal is shown in Fig. 3B. To better compare the deconvolved signal and the PID recordings, 1 s expanded displays of the signals are presented in Fig. 3C showing nearly identical responses to the ethanol fluctuations.

To better compare the frequency responses across multiple trials ($n = 5$ for each frequency), we carried out a cross-correlation analysis of the ETH deconvolved signals with respect to the PID signals during the stimulation (blue) and baseline windows (gray) (Fig. 4). In addition, the auto-correlation of the PID signals within the trials are also presented (red). The mean cross-correlation (solid lines) and individual trials (dashed traces) show strong periodicity with peaks at the period

of the respective frequencies (dashed black lines). There is a consistent small difference in the peak times of the mean cross-correlation with respect to the period across all the frequencies which can be explained by the active suction of the PID. Hence, alcohol sensors can faithfully record ethanol fluctuations up to at least 15Hz.

Ethanol-sensor and PID responses at varying distances from a plume source

To test how distance from the ethanol source and turbulent mixing affected the alcohol sensor reading, we conducted paired PID and alcohol-sensor recordings in a custom-made arena designed to create dynamic odor plumes (Fig. 5A). The recordings were carried out near the source (1), near the middle of the arena (2), and farther downwind (3). Representative traces from the three locations are shown in Fig. 5B. Increasing distance results in a decrease of the amplitude of both the PID and sensor readings. We calculated the correlation of the PID signals from all pair-wise combinations of distinct trials. The distribution of correlation values was near zero, suggesting that on different trials the plumes were highly distinct. In contrast, when we calculated the correlation of PID and deconvolved ethanol signals from the same trial, they were strongly correlated (Fig. 5C). The mean correlations (Mean$\pm$SD: 0.460$\pm$0.175 (1); 0.4708$\pm$0.1584 (2); 0.4343$\pm$0.0937 (3)) between the PID and the deconvolved alcohol signal for the ethanol duration window are presented in Fig. 5D. These correlation values indicate that the ethanol sensors can capture fluctuating signals across a wide range of ethanol concentrations and locations within the arena.

Calcium imaging response onsets coincide with plume contacts detected by the ethanol sensor

We asked whether neural processing in the early olfactory pathways is coincident with sensor recordings by conducting widefield calcium imaging over the dorsal OB of head-fixed Thy1GCaMP6f (GP 5.11) mice (Dana et al., 2014). We paired these recordings with ethanol-

sensor readings during ethanol plume presentations in a wind tunnel specially designed to create dynamic odor plumes. Fig. 6A shows resting fluorescence of the dorsal surface of the OB (left) with the standard deviation of the signal after ethanol plume presentation (right). Ethanol plume presentation resulted in mitral and tufted cell activation, which was observed as patterns of activated glomerular networks. Due to the variable time of arrival of the plume from the valve opening (Fig. 6B), the glomerular responses within each trial were aligned with respect to the sensor-detected ethanol plume (defined as the first peak in the ETH signal after valve opening). Fig. 6C shows the difference in fluorescence traces from 10 different glomeruli for a single trial. Fig. 6D shows the mean activity of six glomeruli from the 10 shown in Fig. 6C, chosen to span a range of response latencies, to 40 different presentations of the ethanol plume. The mean first peak of the ethanol signal detected by the sensor is also presented. As can be seen, the glomerular activity followed and was locked to the plume encounter detected by the sensor.

We next analyzed how the population-level activity in the OB changed following plume contact by performing principal component analysis (PCA) on the population-level activity in the OB. Fig. 6E shows the trajectory of the activity in the first two PCs (accounting for 48% of the variance) after plume detection by the alcohol-sensor. The trajectory after plume detection (blue line with red dots) moves away from the resting state (blue lines alone). The PCA was then carried out on the glomerular dynamics from individual sessions and the Euclidean distance between all the PCs during the resting and post-plume detection was calculated. Fig. 6F shows that the distance between the PCs increased after plume detection during 5 individual recording sessions. These results confirm that the plume detection by the alcohol-sensor is coincident with activation of the projection neurons in the OB.

Behavioral responses to plume contacts in freely behaving mice engaged in odor-guided navigation

To study how plume contacts shape behavior in odor-tracking mice, we trained water-deprived mice to associate ethanol with water. Next, they were tasked to find the ethanol source in a large wind tunnel. Each mouse was equipped with head-mounted sensors and its behavior and ethanol plume contact were recorded. Two instances of a mouse engaged in this task are shown in Fig. 7. Each mouse readily learned to explore the arena and seek the ethanol source (Fig 7A). The deconvolved ethanol signal was correlated with a decrease in speed in freely behaving mice (Fig. 7B, D).

We set defined thresholds for each trial from multiple animals over multiple locations, thus binarizing the deconvolved ethanol signal (see Methods). The trajectories of animals during a window starting 2 s before and ending 2 s after the onset of a contact, defined by the threshold crossing, for a single location are presented in Fig. 8A. In order to make sure that fluctuations within a single contact were not counted multiple times, we limited the analysis to contacts that were separated by at least 5 s from the previous threshold crossing. Furthermore, the animal had to be greater than 10 pixels away from the source at the time of onset to exclude plume encounters near the source. Plume contact was stochastic with varying spatial patterns during different trials (Fig. 8A). In addition, the magnitude of the signal was not spatially predictable. For comparison with random changes in behavior, we randomly selected equal-time sized windows of the trajectories obtained during search without plume contact (defined as sensor reading less than the threshold throughout the duration of the time window). The body speed of the animals decreased upon plume contacts, signified by the white circles, as shown in Fig. 8B. Furthermore, the speed

was lower closer to the source as has been previously suggested by statistical analysis of animal movement (Liu et al., 2020).

The ethanol signal (see Methods), sorted by the distance of the animal from the source at the time of threshold crossing, along with the head and body speed peri-plume contacts (n=177 contacts from 88 trials) are presented in Fig. 8C. The mean $\pm$SEM of the raw ethanol signal and the head and body speeds before and after plume contacts are presented in Fig. 8D. Plume contacts, defined by an increase in the ethanol signal, closely aligned with a decrease in body and head speed of the freely behaving animals (Fig. 8D). The distribution of the mean head and body speeds 1s before and after contact was found to be significantly different ($p = 0.015$ for head speed and $p = 0.0075$ for body speed; Kolmogorov-Smirnov test), while no difference in these distributions was observed for the randomized trajectories ($p = 0.87$ for head speed and $p = 0.785$ for body speed). In addition, the mean speed distributions before plume contact was not different from the randomized trajectory means. Hence, body and head speeds significantly decreased upon plume contact during odor-guided navigation.

Discussion

A growing body of literature has focused on understanding the behavioral strategies for odor-source localization in freely moving mammals (Findley et al., 2020; Gire et al., 2016; Gumaste et al., 2020; Liu et al., 2020). However, correlating real-time olfactory information with behavior and physiological recordings from freely moving animals has been a challenging avenue due to the dynamic nature of the olfactory stimulus. Vickers and Baker (1994) first conducted EAG recordings from antennae mounted on freely behaving moths to correlate odor stimuli with behavior. While EAG is an effective measure to monitor odor information, it suffers from

degradation of signals over time as well as contamination from changes in air pressure and temperature. Another technology routinely used is the PID (Riffell et al., 2008). However, the PID sensor is bulky and heavy, and thus not feasible for monitoring on freely-behaving animals. We therefore used metal oxide gas sensors, specifically alcohol sensors, to monitor real-time olfactory information.

These alcohol sensors are lightweight and inexpensive, and can be easily mounted on the head of freely moving mice. Proximity of the sensor to the nares is critical for making accurate measurements of the signal the animal is sensing. Our paired PID and sensor recordings showed high signal correlation, with nearly identical separation distances as between the sensor and the mouse nares. In addition, fluid dynamics of the ethanol plume in this arena are likely highly correlated across this separation. Furthermore, the results from calcium imaging in OB suggest that the sensor has appropriate sensitivity to detect physiologically relevant fluctuations in ethanol concentrations.

One limitation of using ethanol sensors is their long decay time in response to transient activation. We, therefore, designed kernels resulting from the difference of two exponentials to deconvolve the signal. The deconvolved signals showed a good correlation with the PID responses over time, frequency, and spatial scales. This deconvolution procedure produces similar results as those reported by Martinez et al. (2019). They have also expanded this method to monitor real-time plume detection for mobile robots. We also show good correlation between calcium signals from the mitral and tufted cells in the OB of awake mice and the deconvolved signals from the sensor. In addition, we show that mice reduce both head and body speed in response to odor contacts detected by the sensor. This behavioral change is consistent with that predicted from statistical analyses of mouse behavior during odor-guided navigation (Liu et al., 2020).

There are other limitations to the approach we have taken. The mechanism of detection by the PID is an active process due to a pump that sucks in air, while the metal oxide sensors rely on the adsorption of the analyte to the sensing material, which might account for the shifts we saw in the frequency responses of the ETH signal with respect to the PID signal (Fig. 4), and the difference in the times to reach threshold (Fig. 1E). Also, the PID has a larger dynamic range while the oxide sensor's range is set by the amount of the sensing material, and the adsorption of the analyte. Hence, the saturation of the oxide sensors can occur before the saturation of the PID responses. This could explain the difference in the peak times of the signals generated by the PID and the oxide sensor (Fig. 2B), and in the values of the cross-correlation and the PID autocorrelation (Fig. 4). Still, the periodicity of the cross-correlations shows that metal oxide sensors can detect ethanol at the frequency ranges tested. Furthermore, the decrease in the correlations at 15 Hz can be explained by the reduced time in between the odor pulses for the alcohol sensor to clear the analyte in between the pulses.

Direct calibration of the metal oxide sensors requires generating samples of known ethanol concentration and delivering them faithfully to the sensor. This would necessitate specialized equipment, techniques, and facilities not routinely available in a neuroscience laboratory. While this limitation is valid, we show here that the relative signals from the ethanol sensor show good correlation with the relative signals from the PID, allowing us to rely on this lightweight sensor to record real-time olfactory input to freely behaving animals. In the behavioral arena with the turbulent plume, the signals decrease with the distance from the source while the correlation between the signals, on average, remains constant. An explanation for this phenomenon is that both the PID and the ETH signals degrade equally with the distance; hence, the primary variables dictating the correlation are the distance between the PID and the alcohol sensor, and how thin the

odor filaments are within the turbulent regime. Furthermore, using an improved dielectric excitation method and the resulting impedance measurements from the improved designs, Potyrailo et al. (2020) have shown linear responses to a varying range of concentrations from metal oxide sensors.

We used alcohol sensors for our study so the mice were trained only on a single odor (ethanol) for the behavioral experiments. While this limits the behavioral repertoire, it had the advantage that the animal was tasked to detect only a single molecule. By following our paradigm for oxide sensors that are sensitive to other compounds, this method could be applied to other odors. A recent publication by Williams and Dewan (2020) has reported detection thresholds of mice for aliphatic alcohols about 3 orders of magnitude smaller than the sensitivity of the alcohols sensors, which is in the parts per million range, used here. However, under the conditions of turbulent transport (Celani et al., 2014) employed in our study, odor is transported as high concentration packets (whiffs) interspersed with periods of no odor (blanks). Reaching low concentrations on the scale of the thresholds presented by Williams and Dewan (2020) would occur via diffusion, taking place over larger spatial and temporal scales than in our laboratory setting. Another problem that we encountered during experiments with freely behaving animals is tether management within a large, top-sealed wind tunnel. However, the low power consumption of these sensors allowed us to use ultra-thin wires, reducing impact on animal movement.

Despite these limitations, we envision several extensions of this method. In the future, we plan to combine cameras with actuators in a closed-loop system that would follow the animal and move the wires accordingly. This approach is possible using relatively low-cost components (Fee and Leonardo, 2001; Krynitsky et al., 2020). The small footprint of these sensors can be leveraged to allow us to record the olfactory information arriving at the two nares simultaneously. This can

allow us to assess whether binaral comparison (Findley et al., 2020; Jones and Urban, 2018; Khan et al., 2012; Rajan et al., 2006) informs behavior during plume tracking in freely behaving animals. Additionally, combining these sensors with other sensors that are specific to other chemicals (M. L. Johnston et al., 2012; McGinn et al., 2020) can allow us to study the 'foreground' vs. 'background' problem in the olfactory realm (Riffell et al., 2014).

Our first steps toward measuring real-time olfactory stimuli experienced by a freely behaving rodent will allow detailed quantitative analysis of behavior and provide insights into the behavioral algorithms used to locate an odor source. This technical advance, combined with others for recording or manipulating neural activity in specific brain areas, will help illuminate the brain mechanisms underlying this process that is critical for survival in many species.

Figures

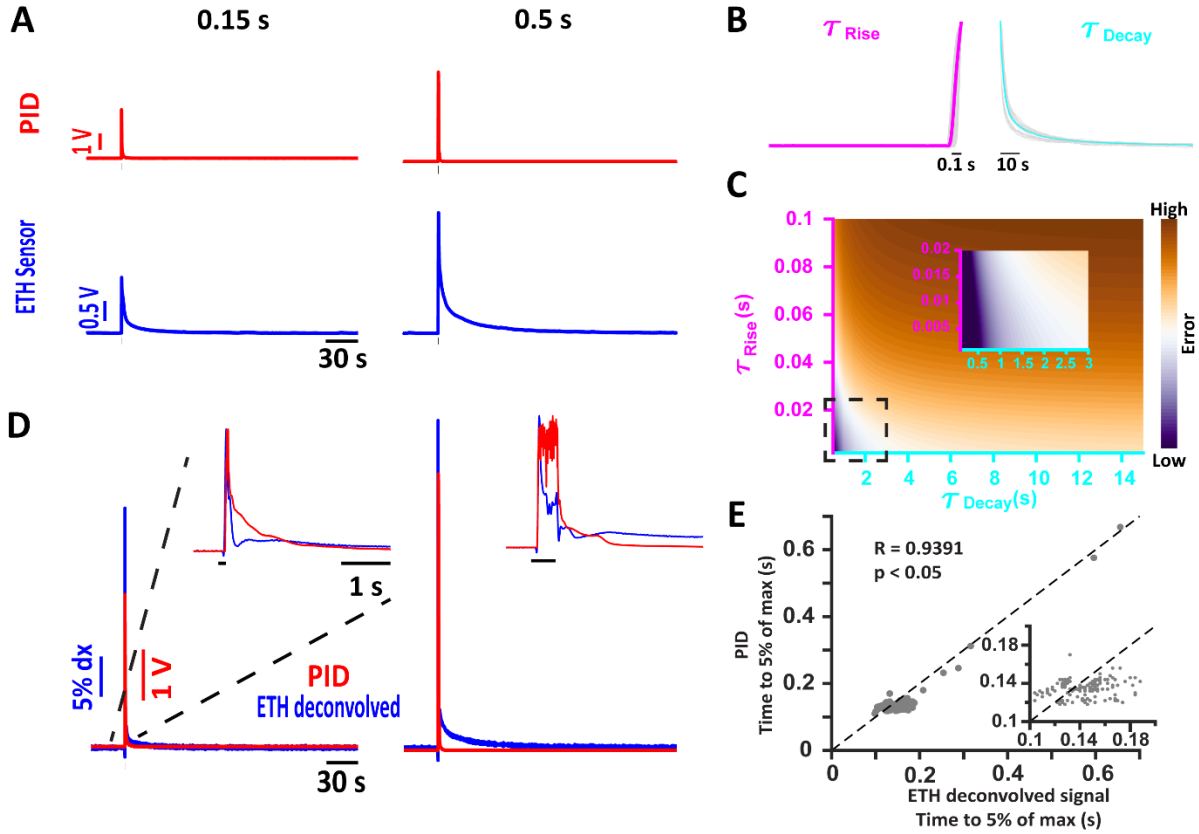

Figure 1. Ethanol sensor response can be deconvolved using a difference of two exponential kernel. A, Representative traces of the PID (red) and the ethanol sensor (blue) response to brief ethanol presentations. The duration of the ethanol pulse is indicated at the top of each column. **B,** Ethanol sensor responses from individual presentations (gray) were averaged to estimate the rise time (τ_{Rise}) to be around 60 ms (magenta) and the decay time (τ_{Decay}) to be around 3.5 s (cyan). **C,** Optimization of the deconvolution kernel by minimizing the mean error between the deconvolved ethanol responses and the PID responses (see Materials and Methods) using a family of kernels with varying τ_{Rise} and τ_{Decay} values. **D,** The deconvolved ethanol signal (blue) from the raw recordings of the ethanol sensor shown in **A** compared with the PID recordings. The inset shows the zoomed-in view of the normalized deconvolved ethanol response and the PID response to

compare the waveforms of the PID response and the deconvolved ethanol signal. The black bar in the inset shows the duration of ethanol presentation. **E,** A linear relation exists between the threshold time (time from the valve opening to 5% of the max) between the deconvolved ethanol signals and the PID responses. Inset shows the zoomed-in view of the cluster of points in the ranges shown.

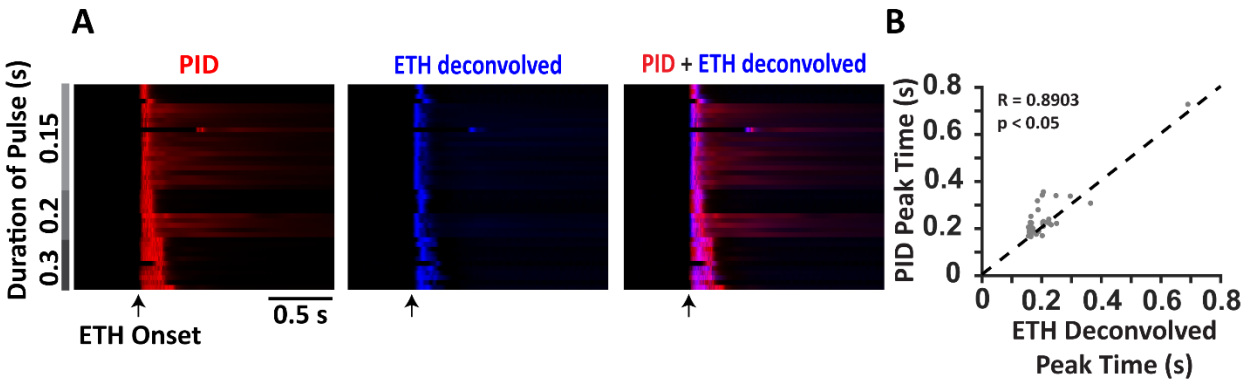

Figure 2. Peak times of the deconvolved ethanol signals coincide with the peak times of the PID responses for brief pulses of ethanol. A, Summary data of PID responses (red; left) and the deconvolved ethanol signals (blue; center) to brief durations of ethanol pulses (shown in gray) presented as a heatmap where each row is a single trial aligned with respect to the valve opening (arrow). Overlaying the deconvolved ethanol signals over the PID responses (right) shows coincidence of the peaks from the two signals (magenta). **B,** Linear relation between the peak times of the PID responses and the peak times of the deconvolved ethanol signals.

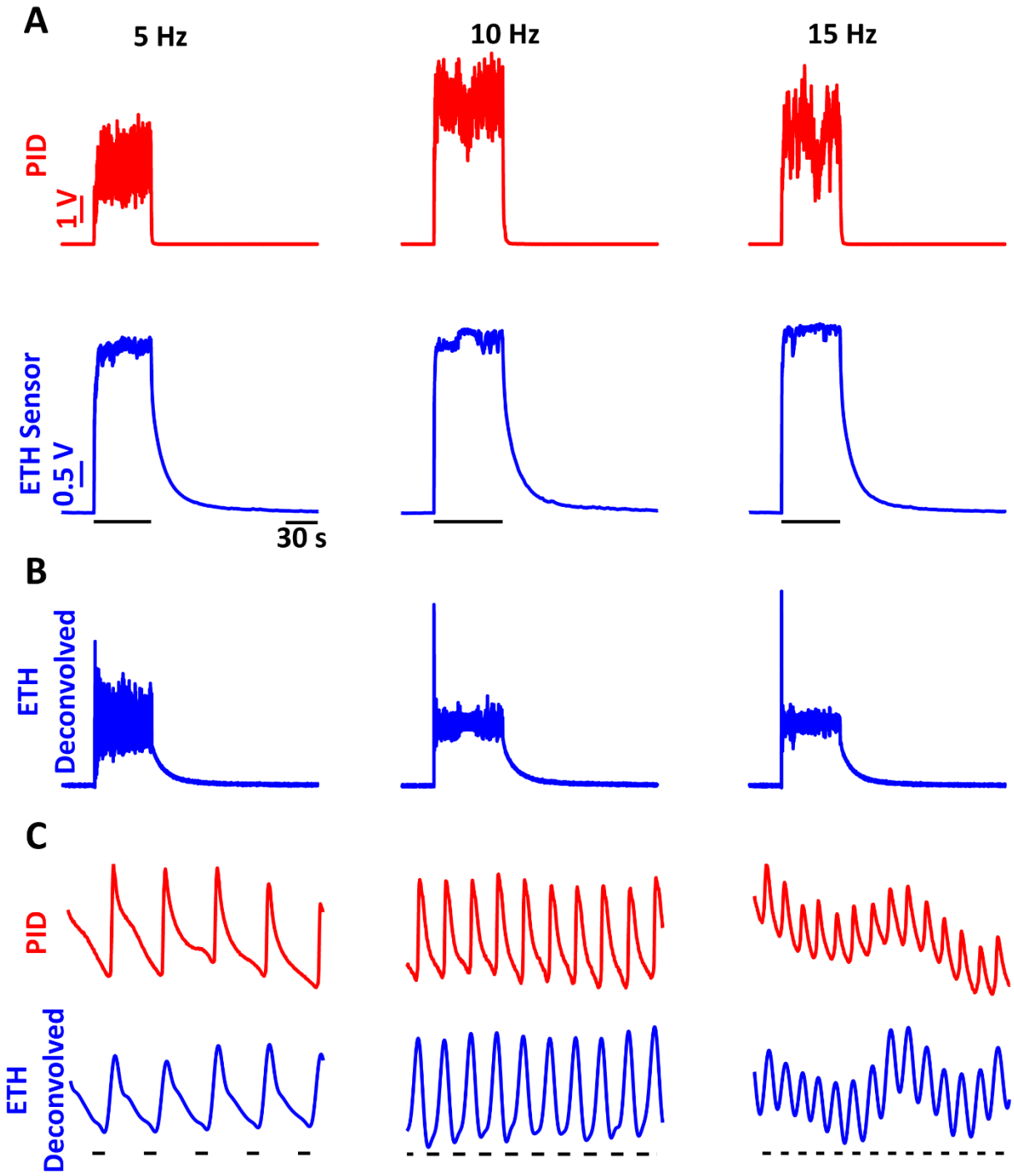

Figure 3. Frequency responses of the ethanol sensor show that the sensor can resolve frequencies of ethanol fluctuations up to 15Hz. A, PID (red) and ethanol sensor (blue) responses to single trials of ethanol fluctuations of 5 Hz (left), 10 Hz (center) and 15 Hz (right) frequencies. **B,** Deconvolved signals of the raw ethanol sensor recordings presented in **A**. **C,** A 1s zoomed-in

view of the PID responses (red) and deconvolved ethanol signal (blue) showing near identical responses in the deconvolved signals and the PID recordings. The black bars underneath the traces indicate the times when the valve was open.

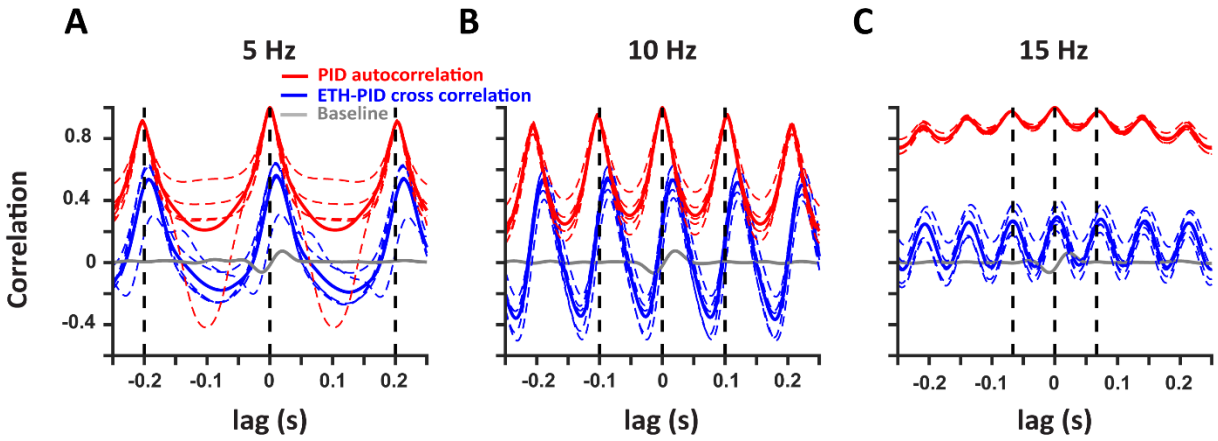

Figure 4. Deconvolved ethanol signals are correlated with the PID signals at multiple frequencies. Cross-correlation of the deconvolved ethanol signal with the PID signal during stimulation (blue) at 5 Hz **(A)**, 10 Hz (**B**) and 15 Hz (**C**) shows robust correlation as compared to baseline (gray). In addition, autocorrelation of the PID signals within each trial are also presented (red). The colored dashed traces represent individual trials and solid traces represent the mean. The black vertical dashed lines indicate the period for each frequency.

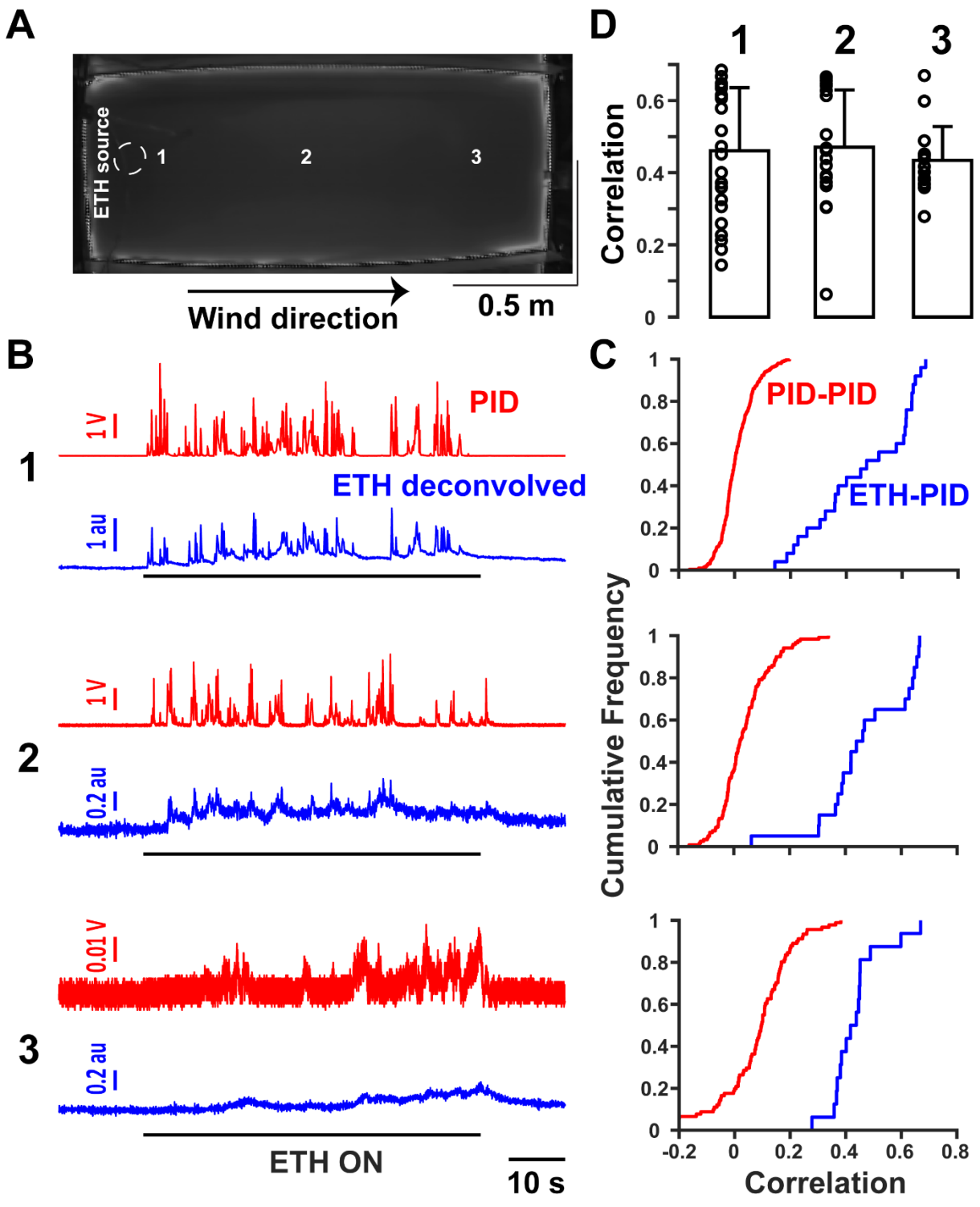

Figure 5. Deconvolved ethanol signals are correlated with the PID responses in turbulent airflow. A, An overhead image of a custom-designed arena (2m(l), 0.9m(w), 0.9m(h)) to create

dynamic odor plumes. The dashed circle represents the location of the source of ethanol port while the arrow points out the wind direction. Also indicated are the approximate locations near the port (1), near the middle of the arena (2), and farthest downwind (3) where paired PID and ethanol sensor recordings were carried out. **B,** Representative traces of the PID (red) and deconvolved ethanol (blue) signals at the locations indicated in **A**. The black bars represent the ethanol stimuli. Notice the changing scales for the amplitude at farther distances from the ethanol port. **C,** Cumulative distributions of PID correlations across pair-wise combinations of different trials (red) vs. correlations between the PID and the ethanol signals within a trial (blue) for the different locations. **D,** Mean+SD correlations (bars) at locations near the port (1), near the middle of the arena (2), and farthest downwind (3) from the ethanol port. Circles are the correlations of individual trials.

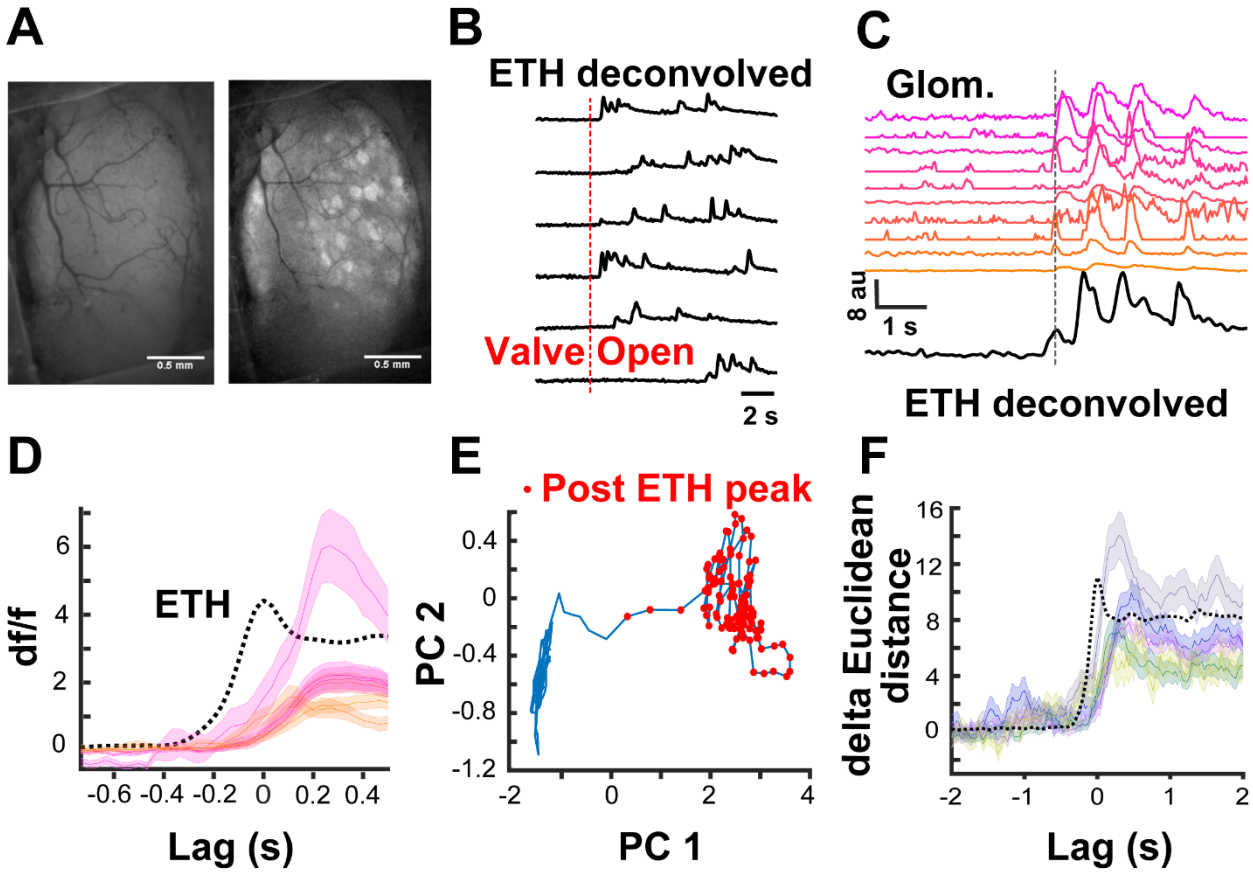

Figure 6. Ethanol plume detected by the ethanol sensor coincide with neural processing in the olfactory bulb. A, A representative cranial window over the dorsal surface of the olfactory bulb of a Thy1-GCaMP6f GP5.11 mouse. Left is at rest while right is the standard deviation image after ethanol plume exposure. **B,** Representative traces showing different times of ethanol plume detection by the sensor after valve opening across six trials. **C,** Calcium traces from 10 different glomeruli aligned to the first peak of the ethanol plume (dashed line). **D,** Mean ± SEM traces from 6 glomeruli averaged over 40 different ethanol plume exposures zoomed in to focus the moment of plume contact. **E,** Movement in the first 2 PC (accounting 48% of the variance) space post ethanol plume exposure from the data presented in **C** and **D**. **F,** Sum of the Euclidean distance from rest across all the PCs aligned to plume detection from 5 different imaging sessions. Each trace is the mean ± SEM across 40 ethanol plume presentations during each session.

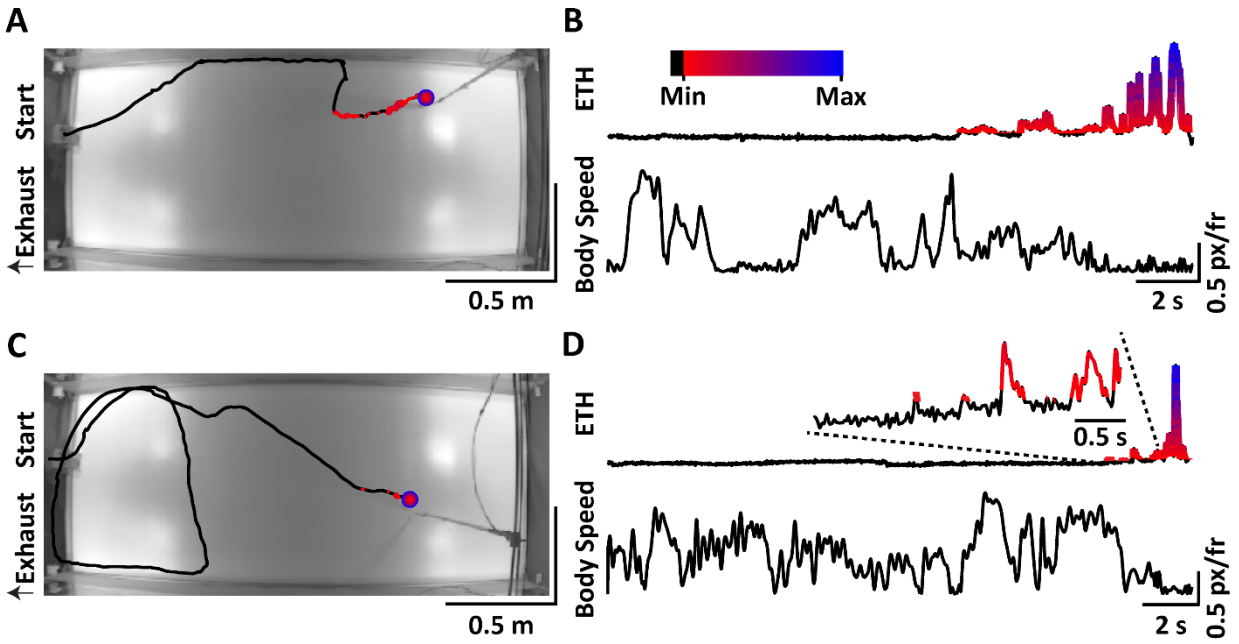

Figure 7. Plume contacts detected by the head-mounted ethanol sensor correlate with behavioral changes in freely behaving rodents. A, An example trajectory of a mouse engaged in odor-guided navigation in our custom-designed arena. Overlaid are the points indicating the locations where plume contacts occurred with the color and size of the points varying by the magnitude of the ethanol plume signal, shown in **B,** measured by the head-mounted sensor. **B,** The deconvolved ethanol signal (top), recorded by the head-mounted sensor, with the body speed (bottom) of the animal over the course of a single trial trajectory, shown in **A**. The plume contacts, set by a threshold, and the magnitude, indicated by the change in color from red (low) to blue (high) are overlaid on the deconvolved ethanol signal. The plume contact is shown to reduce the body speed of the animal. In addition, the plume contact can also be seen to cause a change in the orientation of the animal apparent in **A**. **C** & **D**, Same as A & B but from another trial where the location of the ethanol source is changed. Inset in the top panel of **D** shows the zoomed-in view of the deconvolved ethanol signal within the window indicated by the dashed line.

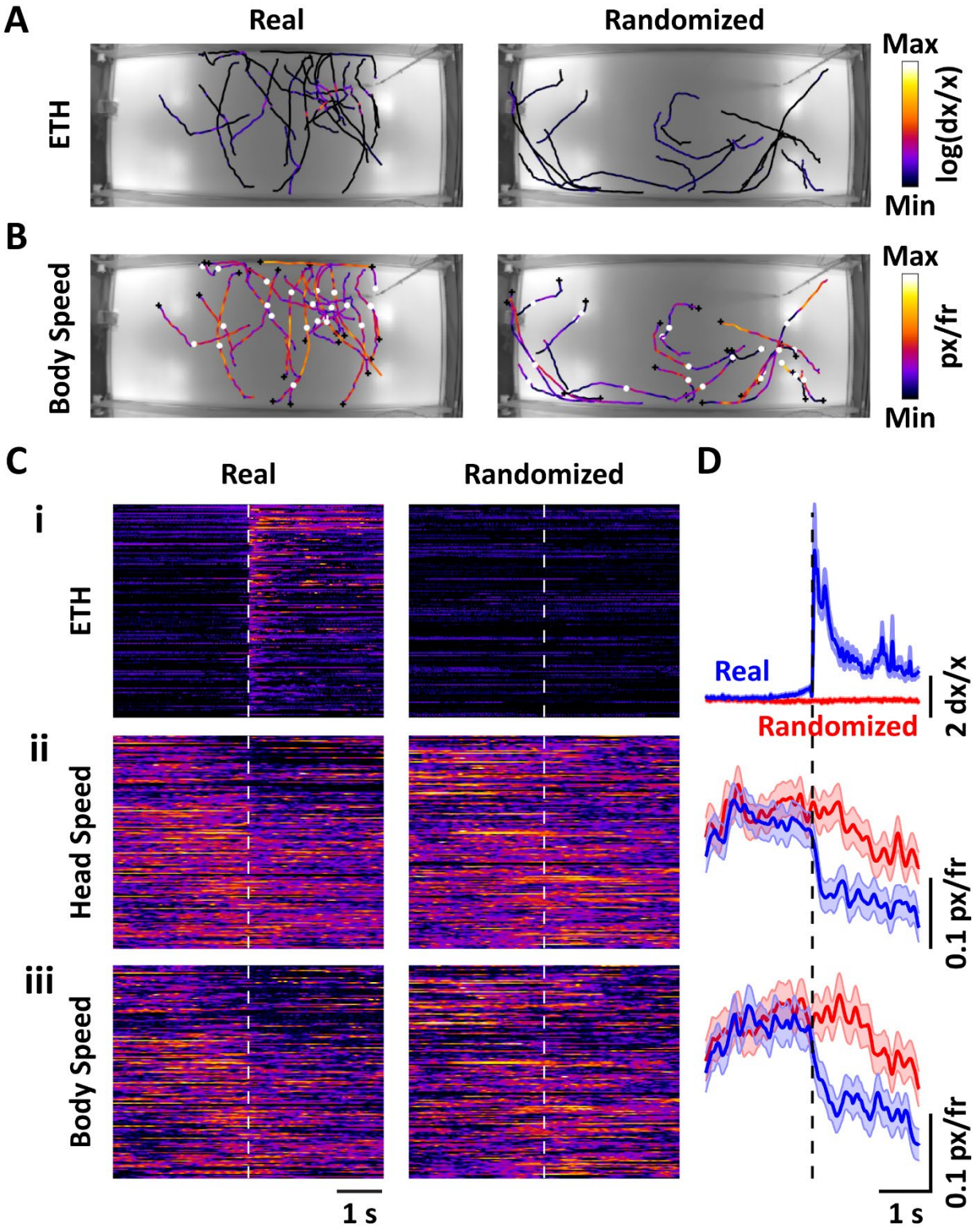

Figure 8. Plume contacts are intermittent and on average are correlated with a reduction in the speed of freely behaving animals. A, Trajectories of multiple animals over different trials

during a 2s period before and after plume contacts for a single ethanol-source location are presented showing that the plume contacts are intermittent and guided by turbulence (left). The color of the trajectories correspond to the log of the deconvolved ethanol signal (see Methods). For comparison, equal time-sized trajectories, randomly selected during the non-plume-contact portion of the trials, are presented (right). **B,** The body speed profile, denoted by the color, peri-plume contacts are presented for the trajectories shown in **A**. Black plus sign is the beginning of the trajectory while the white circle denotes the position at the time of the threshold crossings signifying plume contacts (left). For the randomized (right) case, the black plus sign again denotes the start of the trajectory while the white circle is the position at the middle of the time window. **C,** Heatmaps of the log of the deconvolved ethanol signal (**i**), head speed (**ii**), and the body speed (**iii**) centered around the time of plume contact (dashed white line) sorted by the distance from the source at the time of contact reveal the decrease in the head and body speeds upon plume contacts. For comparison, the randomized heatmaps during the non-plume-contact portion of the trajectories are also presented. Colormap for **Ci** correspond with the colormap in **A**, while colormaps for **Cii** and **Ciii** correspond with the colormap in **B**. **D**, Mean $\pm$ SEM from multiple contacts over different trials and animals, shown in **C**, are presented for the deconvolved ethanol signal (**i**), head speed (**ii**), and the body speed (**iii**), showing clear reduction in the mean head and body speed upon plume contact.

References

Baker KL, Dickinson M, Findley TM, Gire DH, Louis M, Suver MP, Verhagen JV, Nagel KI, Smear MC (2018) Algorithms for Olfactory Search across Species. J Neurosci 38:9383.

Batista-Brito R, Vinck M, Ferguson KA, Chang JT, Laubender D, Lur G, Mossner JM, Hernandez VG, Ramakrishnan C, Deisseroth K, Higley MJ, Cardin JA (2017) Developmental Dysfunction of VIP Interneurons Impairs Cortical Circuits. Neuron 95:884-895.e9.

Celani A, Seminara A (2005) Large-Scale Structure of Passive Scalar Turbulence. Phys Rev Lett 94:214503.

Celani A, Villermaux E, Vergassola M (2014) Odor Landscapes in Turbulent Environments. Phys Rev X 4:041015.

Dana H, Chen T-W, Hu A, Shields BC, Guo C, Looger LL, Kim DS, Svoboda K (2014) Thy1-GCaMP6 Transgenic Mice for Neuronal Population Imaging In Vivo. PLoS ONE 9:e108697.

Fee MS, Leonardo A (2001) Miniature motorized microdrive and commutator system for chronic neural recording in small animals. Journal of Neuroscience Methods 112:83–94.

Findley TM, Wyrick DG, Cramer JL, Brown MA, Holcomb B, Attey R, Yeh D, Monasevitch E, Nouboussi N, Cullen I, Songco J, King JF, Ahmadian Y, Smear MC (2020) Sniff-synchronized, gradient-guided olfactory search by freely moving mice (preprint). Neuroscience.

Gire DH, Kapoor V, Arrighi-Allisan A, Seminara A, Murthy VN (2016) Mice Develop Efficient Strategies for Foraging and Navigation Using Complex Natural Stimuli. Current Biology 26:1261–1273.

Grosek J, Kutz JN (2014) Dynamic Mode Decomposition for Real-Time Background/Foreground Separation in Video. arXiv:14047592 [cs].

Gumaste A, Coronas-Samano G, Hengenius J, Axman R, Connor EG, Baker KL, Ermentrout B, Crimaldi JP, Verhagen JV (2020) A Comparison between Mouse, *In Silico* , and Robot Odor Plume Navigation Reveals Advantages of Mouse Odor Tracking. eNeuro 7:ENEURO.0212-19.2019.

Jackson BJ, Fatima GL, Oh S, Gire DH (2020) Many Paths to the Same Goal: Balancing Exploration and Exploitation during Probabilistic Route Planning. eNeuro 7:ENEURO.0536-19.2020.

Jones PW, Urban NN (2018) Mice follow odor trails using stereo olfactory cues and rapid sniff to sniff comparisons (preprint). Animal Behavior and Cognition.

Justus KA, Cardé RT, French AS (2005) Dynamic Properties of Antennal Responses to Pheromone in Two Moth Species. Journal of Neurophysiology 93:2233–2239.

Khan AG, Sarangi M, Bhalla US (2012) Rats track odour trails accurately using a multi-layered strategy with near-optimal sampling. Nature Communications 3:703.

Krynitsky J, Legaria AA, Pai JJ, Garmendia-Cedillos M, Salem G, Pohida T, Kravitz AV (2020) Rodent Arena Tracker (RAT): A Machine Vision Rodent Tracking Camera and Closed Loop Control System. eNeuro 7:ENEURO.0485-19.2020.

Liu A, Papale AE, Hengenius J, Patel K, Ermentrout B, Urban NN (2020) Mouse Navigation Strategies for Odor Source Localization. Front Neurosci 14:218.

M. L. Johnston, H. Edrees, I. Kymissis, K. L. Shepard (2012) Integrated VOC vapor sensing on FBAR-CMOS array In: 2012 IEEE 25th International Conference on Micro Electro Mechanical Systems (MEMS) , Presented at the 2012 IEEE 25th International Conference on Micro Electro Mechanical Systems (MEMS) pp846–849.

Martinez D, Burgués J, Marco S (2019) Fast Measurements with MOX Sensors: A Least-Squares Approach to Blind Deconvolution. Sensors 19:4029.

McGinn CK, Lamport ZA, Kymissis I (2020) Review of Gravimetric Sensing of Volatile Organic Compounds. ACS Sens.

Monroy JG, González-Jiménez J, Blanco JL (2012) Overcoming the Slow Recovery of MOX Gas Sensors through a System Modeling Approach. Sensors 12:13664–13680.

Pnevmatikakis EA, Soudry D, Gao Y, Machado TA, Merel J, Pfau D, Reardon T, Mu Y, Lacefield C, Yang W, Ahrens M, Bruno R, Jessell TM, Peterka DS, Yuste R, Paninski L (2016) Simultaneous Denoising, Deconvolution, and Demixing of Calcium Imaging Data. Neuron 89:285–299.

Potyrailo RA, Go S, Sexton D, Li X, Alkadi N, Kolmakov A, Amm B, St-Pierre R, Scherer B, Nayeri M, Wu G, Collazo-Davila C, Forman D, Calvert C, Mack C, McConnell P (2020) Extraordinary performance of semiconducting metal oxide gas sensors using dielectric excitation. Nat Electron 3:280–289.

Rajan R, Clement JP, Bhalla US (2006) Rats Smell in Stereo. Science 311:666.

Riffell JA, Abrell L, Hildebrand JG (2008) Physical Processes and Real-Time Chemical Measurement of the Insect Olfactory Environment. Journal of Chemical Ecology 34:837–853.

Riffell JA, Shlizerman E, Sanders E, Abrell L, Medina B, Hinterwirth AJ, Kutz JN (2014) Flower discrimination by pollinators in a dynamic chemical environment. Science 344:1515.

Vickers NJ, Baker TC (1994) Reiterative responses to single strands of odor promote sustained upwind flight and odor source location by moths. Proc Natl Acad Sci USA 91:5756.

Wang C, Yin L, Zhang L, Xiang D, Gao R (2010) Metal Oxide Gas Sensors: Sensitivity and Influencing Factors. Sensors 10:2088–2106.

Williams E, Dewan A (2020) Olfactory Detection Thresholds for Primary Aliphatic Alcohols in Mice. Chem Senses 45:513–521.

Dynamics of odor-source localization: Insights from real-time odor plume recordings and head-motion tracking in freely moving mice

Mohammad F. Tariq[1,2], Scott Sterrett[1,2], Sidney Moore[2], Lane[2,4], David J. Perkel[3], David H. Gire[2]

[1]Graduate Program in Neuroscience, [2]Department of Psychology, [3]Departments of Biology & Otolaryngology, University of Washington, [4]Department of Psychology, Seattle University

Abstract

Animals navigating turbulent odor plumes exhibit a rich variety of behaviors, and employ efficient strategies to locate odor-sources. A growing body of literature has started to probe this complex task of odor-source localization to further our understanding of neural encoding and decoding of naturalistic sensory stimuli. However, correlating the intermittent olfactory information with behavior has remained a long-standing challenge due to the stochastic nature of the odor stimulus. We recently reported on a method to record real-time olfactory information available to freely moving mice during odor-guided navigation, hence overcoming that challenge. Here we combine our odor recording method with head-motion tracking to establish correlations between plume encounters and head-motion changes. We show that mice exhibit robust head-pitch motions in the 5-14Hz range during an odor-guided navigation task, and that these head motions are modulated by plume encounters. Furthermore, mice orient towards the odor source upon plume contact. Head motions may thus be an important part of the sensorimotor behavioral repertoire during the naturalistic odor source localization.

Introduction

Animals exhibit rich sensorimotor transformations as part of their natural behavior. Studying naturalistic behaviors in rodents (Dennis et al., 2021) offers the opportunity to understand the neural circuits involved in processing sensory information for goal-directed behaviors. For example, odor plume-guided navigation is a tractable system in this pursuit, but has historically been under-studied due to the inability to experimentally monitor the complex odor plumes (Ackels, 2022; Marin et al., 2021) that rodents encounter during free behavior. Lewis et al. (2021) and Ackels et al. (2021) have shown that the olfactory bulb of mice can certainly encode the fast dynamics present in a naturalistic plume, but how this neural activity shapes behavior in response to intermittent plume encounters during naturalistic behaviors have not been clearly established.

Vickers and Baker (1994) first precisely correlated plume contacts to behavior in freely flying moths. Their seminal work, along with subsequent studies (Cardé and Willis, 2008; Mafra-Neto and Cardé, 1998, 1994; van Breugel and Dickinson, 2014; Vickers, 2000; Vickers et al., 2001) revealed robust behavioral sequences exhibited by invertebrates during the complex odor-source localization task. Recently, Demir et al. (2020) have shown important behavioral changes in response to turbulent plume encounters for walking flies navigating a complex olfactory landscape.

Mammalian responses to plume encounters during airborne odor tracking have not been established. Findley et al. (2021) have recently shown head motions as a key behavioral feature during a two choice task, where the directional choice was dependent on the intensity of the odor. However, the plume encounter-dependent changes in rodent head motions were not established in their study. In addition, Liao and Kleinfeld (2023) have shown alterations in behavioral states of freely moving rats engaged in an exploratory behavior. They, along with Findley et al. (2021),

have also established important correlations between rodents' sniffing and their head motions. We have previously used metal oxide sensors to record real-time olfactory information during airborne odor-tracking in mice (Tariq et al., 2021). Here we combine this method with head-mounted accelerometers to study how head motions change around plume encounters.

Like Findley et al. (2021), and Liao and Kleinfeld (2023) we show head motions as a critical component of the mouse natural behavioral repertoire. We extend upon these findings by establishing that plume encounters in a turbulent setting modulate these head motions. In particular, we show that preceeding plume contacts mice increase the amplitude of their head-pitch motions in the active search band (5-14 Hz), which reduces greatly right after the contacts. In addition, mice also switch from rearing to foraging after plume contacts, with a corresponding increase in the frequency of the head-pitch motions and decrease in the body angle with respect to the source. Our results then suggest that mice are able to decipher the relative location of the source with each plume contact. Similar head motions are also involved in a visually-guided task (Michaiel et al., 2020), which points to the importance of head motions for sensory acquisition and motor guidance during free behavior. Hence, our work combined with that of Findley et al. (2021) lay the groundwork to study the neural mechanisms underlying sensorimotor transformations during the naturalistic behavior of odor-plume tracking in mammals.

Materials and Methods

Animal Housing and Protocol

All animal procedures were approved by the University of Washington Institutional Animal Care and Use Committee. Wild type mice of both genders (n=7; 3 females/4 males), obtained from The Jackson Laboratory (Strain #000664) were used as test subjects. Mice were

maintained on a reverse 12 hrs light schedule (7AM lights off; 7PM lights on). After surgery, described below, each mouse was housed individually.

Surgery

All the mice were between 19-24 weeks of age at implantation. Each mouse underwent aseptic surgery for implantation of a 3D printed part, housing the female end of PCB connectors (Mill-Max 833-93-100-10-001000; 2 rows of 3 pins). The 3D part was affixed to the skull with cyanoacrylate. A 1-mm screw was also implanted over the caudal skull on top of cerebellum to anchor the part. The glue was then built around the part and the screw to ensure long-term stability of the part. The exposed area of the skull was covered with dental cement. After each surgery, the mouse was monitored for 45 minutes in a bedding and chips free cage until the mouse was mobile again. The mouse was then housed individually and monitored for 10 days after surgery for post-surgery complications. Analgesics, Carprofen and Lidocaine topically applied, were administered before the surgery. Post-surgery carprofen was administered if needed.

Behavioral training and task

After a >2weeks post-surgery period, the mice were water-restricted and trained to associate the smell of ethanol with water. This was achieved by placing weigh boats containing water and ethanol-soaked pads taped underneath in the home cage. Each mouse was given approximately 15 minutes to consume the water from the weigh boat. The behavioral apparatus and the task design for odor-source localization were as previously described (Tariq et al., 2021). Briefly, the odor port in the custom-designed arena was placed randomly in an x-y location and the goal for the mouse was to locate the source of the odor port to receive reward (water droplet). A 1-s tone of 1 kHz signified the end of the trial. After each trial was completed, the mouse was

coaxed back into the housing cage located outside the arena, and the odor port was repositioned for the next trial. The order in which the mice were tested was randomized for each day.

The arena was illuminated using infrared lights to remove visual cues, and the behavior was recorded using an overhead camera (Basler acA640-90uc). In addition, white noise was continuously played in the room to mask any acoustic cues. To minimize strain by the cables, a linear actuator (Progressive Automation PA-15), with a slip-ring commutator mounted on a small plexiglass sheet, to minimize noise, was installed in the arena. The actuator motion was manually controlled by an experimenter with a switch, located outside the arena, based on the location of the mouse within the arena. Each mouse was weighed before water restriction to establish the baseline weight and was then maintained at a weight >0.85 times the baseline weight. In addition to the behavioral task, the mice were supplemented with water following the same protocol as the ethanol-water association, described above, to maintain their body weight.

Head-mounted odor sensor and accelerometer

A Figaro TGS 2620 sensor, as described previously (Tariq et al., 2021), mounted on a custom-designed PCB was used to record the real-time olfactory information. Also mounted on the PCB was a 3-axis accelerometer (Analog Devices ADXL 335). The orientation of the accelerometer with respect to the ground can be seen in Figure 1A. The accelerometer and the ethanol sensor were respectively powered by 3.3V and 5V outputs from an Arduino (Adafruit), and shared a common ground. The PCBs were screwed onto a 3D printed part using miniature screws (McMaster-Carr#96817A704) and the part also contained male PCB pins to connect with the 3D printed part glued onto the mouse skull. A 30 Gauge, 8 conductor cable (McMaster-Carr#3890N21) was soldered directly onto the PCB for signal conduction. The outer insulation jacket was removed from the cable to make it more flexible to facilitate mouse locomotion. The

data were digitized using a National Instruments NI6212 DAQ, and acquired and stored using LabView scripts. To acclimate the mice with the 3D printed part, a bare part without the PCBs mounted was connected to the head piece after the odor-localization behavioral task each day. In addition, before the odor-localization task in the arena, a smaller version of the apparatus was used to acclimatize the mice with the head-mounted sensors in a bedding-free mouse cage.

Signal Analysis

All the time-series analysis was done prior to analyzing the position data to minimize the location bias. Furthermore, the training for DeepLabCut (DLC) (Mathis et al., 2018; Nath et al., 2019), described below, was conducted by a researcher not involved in the data collection.

Head-mounted Sensors

All analysis code was written in MATLAB R2019a (MathWorks). The ethanol sensor signal was low-pass filtered (5Hz cutoff) and then deconvolved using a difference-of-two-exponentials kernel with τ_{Rise} and τ_{Decay} values set at 0.02 and 10s, respectively (Tariq et al., 2021). For plume-event detection, the slope of the cumulative sum of the signal around all time points was calculated for 1-s segments before and after that point. The onset of an event was defined as the time point when the ratio of the forward and reverse slopes crossed a threshold. The threshold was determined by pooling data from all of the odor-localization task sessions, and sessions involving the presentation of a plume without an animal running in the arena. This allowed us to minimize spurious detections that might result from the wind as temperature changes affect the signal over longer time scales. Events that were separated by greater than 5s were pooled for the group data. The accelerometer readings were calibrated before and after running animals by placing the head piece in various orientations. The voltage recordings from the accelerometer were converted to units of g by zeroing and scaling appropriately. The recordings were then low pass

filtered (20Hz cutoff), and the derivative of the signals was taken to convert the acceleration to jerk (Karalis and Sirota, 2022). The resulting jerk signal was then used for time-frequency analysis via the *cwt* (Continuous Wavelet Transform) function. For rearing and foraging determination, a 1-s moving median of the Z- and X- axes was calculated. The median signal for the X-axis was then subtracted from the Z-axis. The data from all the animal trials were then pooled and a three Gaussian model was then fit to the distribution as shown in Figure 3A using a Gaussian Mixture Model algorithm (MathWorks File Exchange; Matthew Roughan Commit Date: 2007). This analysis was based on the work of Liao and Kleinfeld (2023). To determine the dominant frequency of head-pitch motions, the band with the highest power within the active search (5-14 Hz) was used. The real trajectories were defined as the time-window around the onset of events (described above), while random trajectories were obtained by randomly selecting equal time-sized windows throughout the trial, except for 1-s windows on either side of real events.

Position Data

We used DLC to train a deep neural network for mouse position tracking. Trial videos were cropped to the size of the arena. The neural network was trained with videos from recorded trials without wire occlusion to reduce external artifacts. We tracked mouse nose, left ear, right ear, neck, center of mass (i.e., center of torso), and tail base; additionally, we tracked the port location as well as the corners of the arena. Each frame within a given trial therefore had 11 corresponding x,y coordinates with a respective likelihood value (range [0-1]), which is the calculated certainty evaluated by DLC. Our trained neural network exhibited a test error of 2.33 pixels, satisfying the reported standard for human level accuracy of 2.7 pixels (Nath et al., 2019). We then developed a MATLAB (2022b) package to aggregate and analyze the position data alongside the existing accelerometer and ethanol sensor datasets. DLC output was used for angle calculations. To

calculate the body angle, the mid-point between the neck and body coordinates was determined. Then the angle between the vector connecting the mid-point with the body, and the vector connecting the mid-point to the port was defined as the body angle w.r.t. the port. The direction of the angle was taken as positive if the body to mid-point vector was clockwise to the vector connecting the mid-point to port, and negative when it was counter-clockwise. The head angle was defined as the angle between the vector connecting nose with neck, and the vector obtained by a 180° rotation of the vector connecting neck with body. Hence, an egocentric right head turn was thus considered negative while a left head turn was considered positive. To minimize noise due to erroneous DLC labeling, any of the labels with a likelihood less than 0.9 was set to NaN, removing those points from the calculation. The angles were analyzed using the MATLAB circular statistics toolbox (Berens, 2009). In addition to the time criteria (described above), only events greater than 15 pixels from the source, approximately the length of an adult mouse, at the time of encounters were pooled together for the group data.

Results

To understand the plume-encounter dependent changes in mouse head motions during an airborne-odor source localization, we combined our previously published method of recording real-time plume information (Tariq et al., 2021) with head-motion monitoring using a 3-axis accelerometer.

Concurrent head-motion tracking with real-time plume information during odor-guided navigation task

Figure 1A shows the 3D part designed to carry the PCB with the ethanol sensor and accelerometer. The location of the accelerometer and the sensor with respect to the mouse nose is

approximately the same as it would be in real life. This device then allowed us to record the real-time plume information experienced by, and head motions of a mouse engaged in odor-guided navigation. An example trial is presented in Figure 1B, while the accelerometer reading, speed, and olfactory information experienced by the mouse during that trial is presented in Figure 1C. To better visualize the evolution of the signals over time and space zoomed-in views around the encounters labeled in Figures 1B and C are presented in Figure 1D. Hence, this method allowed us to look at how the head motions of mice engaged in the odor-localization task change with each odor-plume encounter.

Plume encounter-dependent changes in the amplitude of the mouse head-pitch motions

To better characterize how plume encounters affect the head-pitch motions, we took the derivative of the X-axis read out from the accelerometer to convert the acceleration to jerk (Karalis and Sirota, 2022). Since the X-axis is aligned with the direction of gravity, this channel was the most useful for studying the up and down (pitch) motions of the mouse head. It was readily apparent that the pitch motion had many frequency components embedded in the signal, as previously reported (Findley et al., 2021; Liao and Kleinfeld, 2022). We therefore aligned the jerk signals with respect to the onset of plume encounters shown in Figure 2C, and conducted time-frequency analysis using the CWT of the jerk signal as shown in Figure 2D. The prominent frequency band was found to be in the 5-14 Hz range. Interestingly, this frequency band was also prominent during the non-plume encounter portions of the trajectory as shown by the randomly selected trajectories (middle panel; Figures 2C-E). This is in line with previously published work (Karalis and Sirota, 2022).

To better characterize how the amplitude of head-pitch motions evolve over time, and in particular around plume encounters, we examined the power within the active search band (5-14

Hz) over time presented in Figure 2E. In addition, the power from the example trial presented in Figures 1B-D is presented in Figure 2B. As seen in Figure 2E, there is a rapid increase in the amplitude of pitch motions immediately before plume encounters, which decreases rapidly soon after plume encounters. Thus, mice move their head up and down more vigorously before plume encounters, and slow these motions following an encounter.

Mice switch from rearing to foraging after plume encounters

Liao and Kleinfeld (2023) have shown that rats engaged in free exploration switch from rearing to foraging, and that the sniff frequency during the foraging and rearing epochs are different. To test if such a switching also occurred during our task, we examined the difference between moving medians of the Z- and X-axes. We acknowledge that this is an indirect method to look at the relative angle of the head with respect to the ground, but that is a technical limitation of using accelerometers. The distribution of this difference across all animals is presented in Figure 3A. This distribution was then fit to a sum of three Gaussians (black dashed curve) and the third Gaussian (magenta) was then used to establish the threshold for rearing. We next looked at the dominant frequency of head-pitch motions during these epochs shown in Figure 3B. The leftward shift of the dominant frequency during rearing is consistent with that observed by Liao and Kleinfeld (2023), however, our effect is not as strong as they observed. While we cannot directly ascribe the frequency of head pitch motions with sniffing in our paradigm, many groups (Findley et al., 2021; Karalis and Sirota, 2022; Liao and Kleinfeld, 2022) have established a strong correlation between sniffing and rodent head pitch motions. Furthermore, to study the plume encounter-dependence on rearing and foraging we looked at this difference measure over time for the trajectories presented in Figures 2C-E. As shown in Figure 3C, there is an increase followed by a decrease right around plume encounters, suggesting that

the mice switch from rearing to foraging upon plume contacts. This switch is also accompanied with a corresponding increase in the dominant frequency of the head pitch motion as shown in Figure 3D.

Mice reduce their body angle with respect to the source upon plume encounters

We next asked if mice can predict the location of the source with each plume encounter. To answer this question, we calculated the body angle with respect to the source (see Methods). Figure 4A shows the body angles of the mouse over time for the trajectories presented in Figure 1D. It was apparent that the mouse reduced the variability of its angle with respect to the source after plume encounter. To further quantify this effect, we calculated the mean angle of each trajectory 3s before and after the encounter, and then calculated the difference between the instantaneous angles and the mean angles for that time period. Figure 4B shows the probability heatmap over time for this angular difference for the real (blue; top) and random (red; bottom) trajectories. The distribution of the difference angles for the real trajectories becomes narrower (blue) after plume encounters than before encounters (gray), as can be seen in Figure 4C. No such change is observed for the randomly selected trajectories (Figure 4C bottom; $p = 0.0002$ real & $p = 0.6383$ randomly selected trajectories; Paired Wilcoxon signed rank test). Furthermore, the mean angle over time reduces after plume encounter, as can be seen in Figure 4D with a corresponding increase in the strength of the resultant vector for real (blue) trajectories. The mean angle for the randomly selected trajectories (red; Figure 4D top), on the other hand, hovers around 10° (close to no particular direction preference with respect to the source). Furthermore, the vector strength for the random trajectories (red; Figure 4D bottom) is close to 0.5, signifying the angles are randomly spaced equally around the mean angle.

Plume encounters reduce mice head yaw angle variability

While casting downwind of an odor source has been established as an efficient navigation strategy for flying insects (Mafra-Neto and Cardé, 1998, 1994; Vickers and Baker, 1994), to date such a type of strategy has never been established for walking mammals engaged in odor-source localization. We therefore looked at the head yaw angles as a correlate of casting. Figure 5A (top) shows the mean angle over time for the real (blue) and randomly selected (red) trajectories. While the mean angle for the real and randomly selected trajectories do not differ after plume encounters, there is a slight increase in the strength of the resultant vector (bottom) for real trajectories as compared to the random. This increase in strength for the real trajectories suggests that variability around the mean angle decreases peri-plume encounters. In addition, the probability heatmap over time before (grey) and after (blue) plume encounters is presented in Figure 5B, with the distribution presented in Figure 5C.

Discussion

Correlating sporadic plume encounters to behavioral changes, and neural recordings during odor-guided navigation has remained elusive (Ackels, 2022; Marin et al., 2021) due to the constraints in real-time olfactory monitoring. We previously reported on a method to record the odor information available to a freely moving mouse using head-mounted sensors (Tariq et al., 2021). Here we combined this method with head-motion tracking using accelerometers to study how plume encounters shape head motions during an odor-localization task.

We show that mice actively search for olfactory plume encounters in our odor-source localization task by exhibiting robust head-pitch motions in 5-14Hz range. These head motions are increased in their amplitude just before the plume encounter, and robustly decrease right after

the encounter. This, in conjunction with our previous result of decrease in speed of locomotion after plume encounters suggest that the decrease in the head-pitch motion might be a strategy to localize the odor source. The increased vigorous head motions before encounter could be to catch a whiff of the plume, while the slowing of the head-pitch motions could be to decipher the location of the source.

Hence, when we looked at the direction of the motion after plume encounters by calculating the body angle with respect to the source, we find that mice maintain their mean angles after plume encounters and reduce their angles with respect to the source. This finding suggests that mice are able to extract location information from each plume encounter. We also show that mice switch from rearing to foraging after plume encounters, with an increase in the frequency of the head motions. This switching from rearing to foraging is consistent with switching to sampling the air vs. sampling closer to the ground as an effective navigation strategy for a computational searcher (Rigolli et al., 2022). In addition, we show that the yaw head angles are reduced in their variability after plume encounters.

Figures

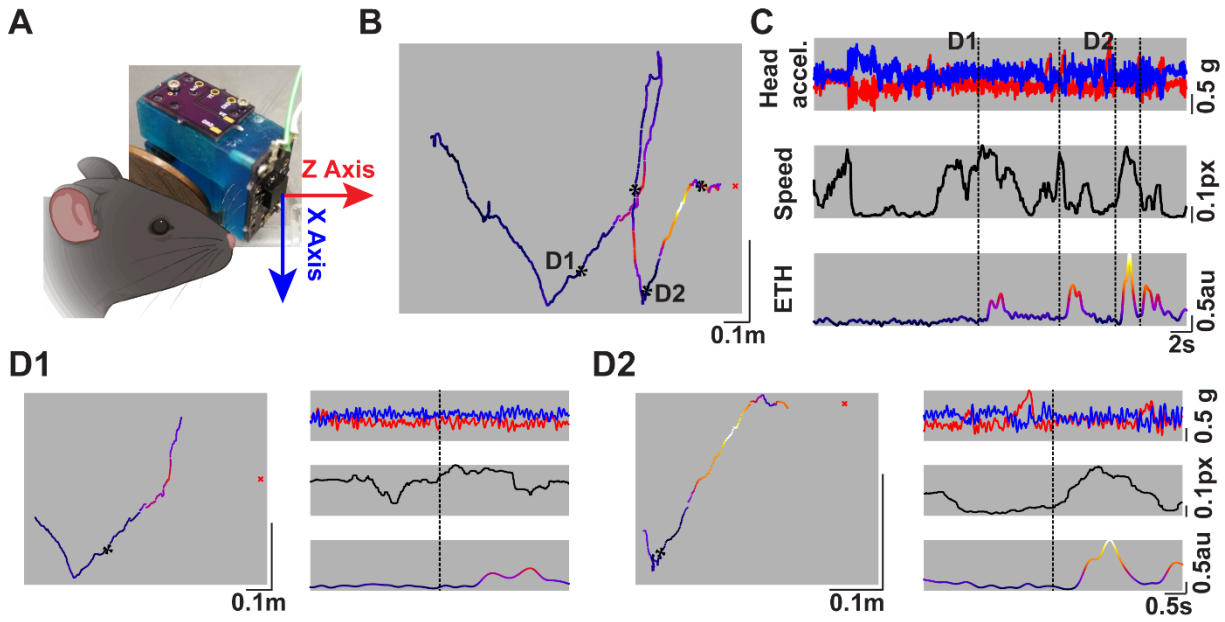

Figure 1. Concurrent head-motion tracking with real-time odor plume monitoring. A) The designed 3D-printed part with the custom designed PCB to monitor the plume information along with an accelerometer. The arrows correspond to the axis of orientation of the accelerometer and the color correspond with panel **C. B)** An individual trajectory of a mouse engaged in plume-tracking to locate the odor source for a water reward. Overlaid on the trajectory is the colormap of the real-time plume signal experienced by the mouse. The black asterisks represent the locations of plume encounters (as defined by our algorithm). The red "x" marks the location of the odor source. **C)** (Top) The read-out over time from the Z- and X- axis channels of the accelerometer (red & blue, respectively) from the trajectory shown in **B**. (Middle) The speed of the animal over time during the trial shown in **B.** (Bottom) The plume signal experienced by the mouse during its search. The color-scale goes from dark (low signal) to lighter (higher signal) and corresponds with the colors shown in **B**. Black dashed lines represent the times of plume encounters. **D1)** A 3-s (before and after) window showing the position (left) and time (right)

evolution of the signals around the encounter labeled as **D1** in **B** and **C**. **D2)** Same as **D1** but for the encounter labeled as **D2** in panels **B** and **C**.

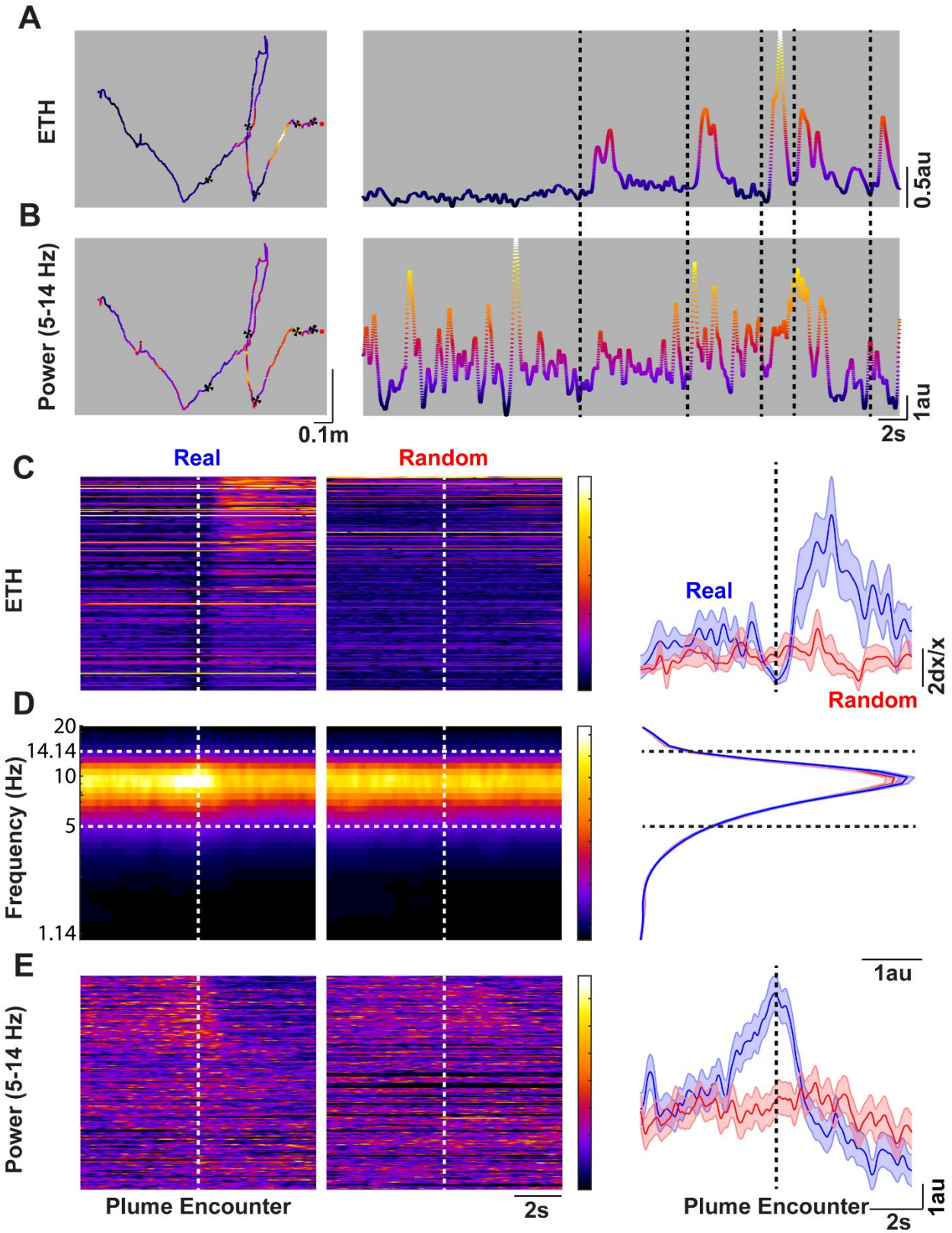
A
ETH
0.5au
B
Power (5-14 Hz)
0.1m
1au
2s
C
Real
Random
ETH
Real
Random
2dx/x
D
20
14.14
10
5
1.14
Frequency (Hz)
E
Power (5-14 Hz)
Plume Encounter
2s
1au
Plume Encounter
2s
1au

Figure 2. Plume encounters are preceded by increased amplitude of head-pitch motion in the active search (5-14 Hz) band, and immediately followed by decreased head-pitch motion. A) Same trajectory with the plume signal overlaid over space (left), and over time (right) as depicted in Figures **1B-D**. **B)** Amplitude of the mouse head-pitch motions in the 5-14 Hz band (see panel **D**) during the search shown in **A** over location (left) and time (right). The black asterisks, and dashed lines represent the locations and times when plume encounters occurred. **C)** Group data showing the heat map of the plume signal in a 5-s window before and after a plume encounter for real (left) and randomly selected portions (middle), while the mean±SEM of the all the encounters' and random trajectories' plume signals (Real: blue; Random: red) over time is presented (right). The signals in the left and middle heatmaps are sorted by the distance of the animal from the source when the encounter happened (Top: closest). **D)** A 5-s window (before and after plume encounter) CWT of the derivative of the accelerometer pitch motion showing 5-14 Hz predominant band (demarcated by the white dashed lines), referred to as the active search band, during real (left), and randomly selected trajectories (middle). The color scales are the same for the spectrograms for real and randomly selected data. In addition, mean power over the frequency bands are presented (right). Black dashed lines again demarcate the 5-14Hz band. **E)** The time-evolution of the power in the active search band during real (left) and randomly selected (middle) trajectories. The sorting of the signal is the same as in **C**. Furthermore, the color scale is the same for both heatmaps. Mean±SEM (right) of the power in the active search band over time is also presented.

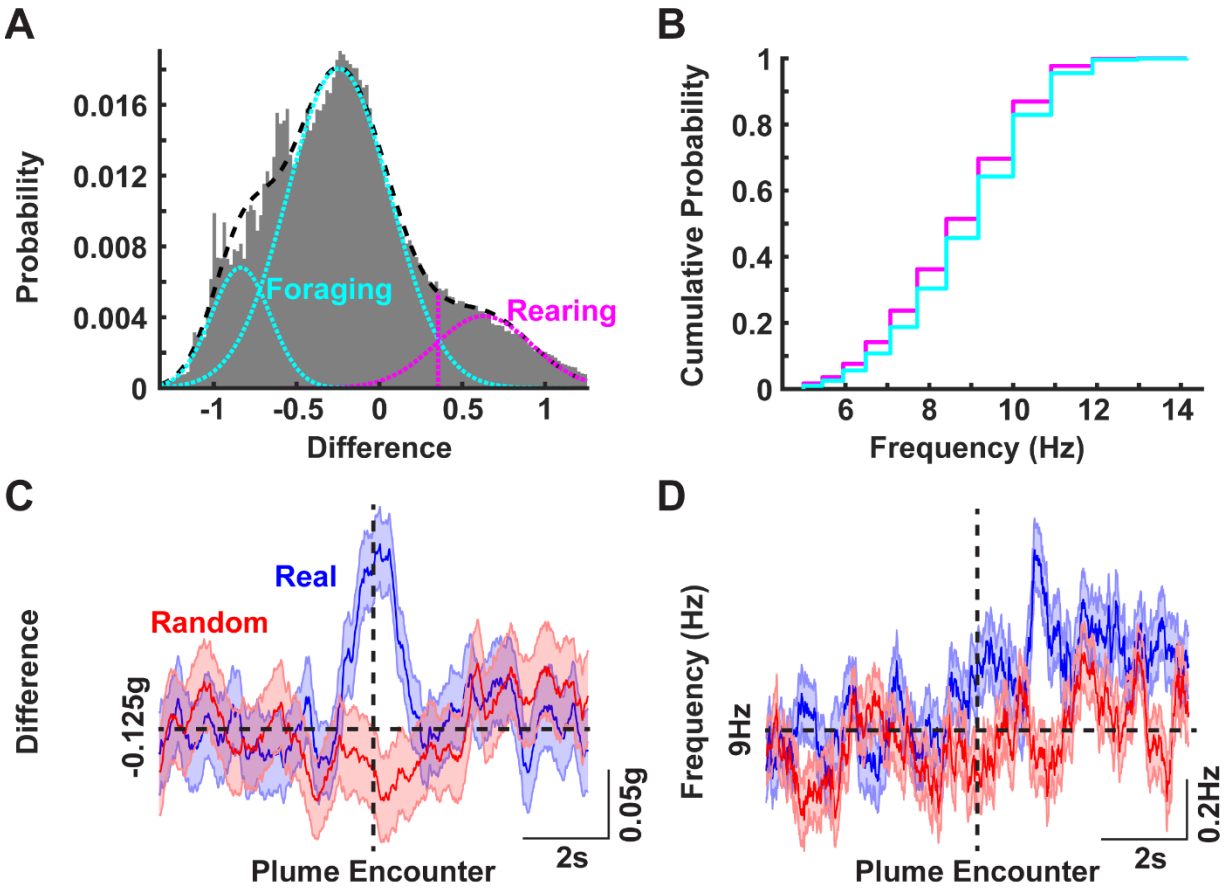

Figure 3. Plume encounter results in a switch from rearing to foraging with a corresponding increase in the frequency of head-pitch motion. A) The difference in the median Z- and X-axes read out from the accelerometer pooled over all trials and all animals. The resulting distribution was then fit with the sum of three Gaussians (black dashed curve). The mean-S.D. (magenta dashed line) of the third Gaussian (magenta curve) was then set as a threshold to classify the behavior as either rearing or foraging. **B)** Cumulative histograms of the dominant frequency of head-pitch motion in the active search band during the rearing (magenta) and foraging (cyan) epochs. A leftward shift is apparent during rearing events. **C)** Mean ± SEM of the difference of median of Z- and X-axes readings around real (blue) and randomly selected (red) trajectories (same plume encounter events as those presented in Figures **2C-E**). **D)** Mean ±

SEM of the dominant frequency of the head-pitch motions around plume encounters for real and randomly selected trajectories.

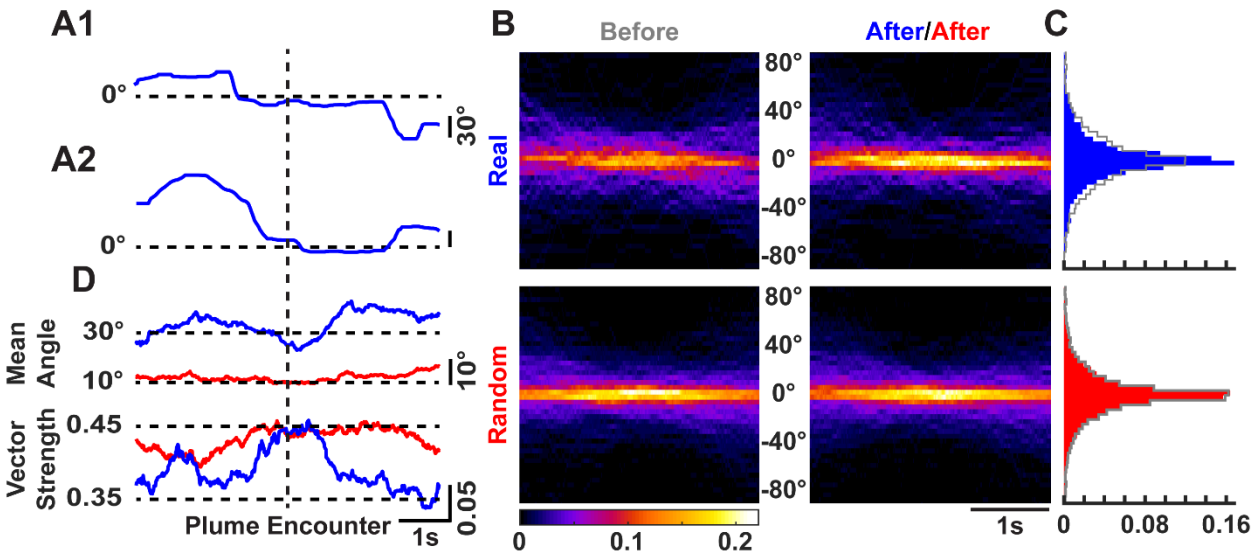

Figure 4. Mice reduce their body angle with respect to the odor source upon plume encounter. A1) The body angle (see Methods for description) of the mouse with respect to the odor source during the trajectory **D1** shown in Figure **1**. **A2)** Same as **A1** but for the trajectory **D2** in Figure **1**. **B)** The probability heatmap of the angle difference between instantaneous angles and the mean angle 3s before (gray) and after for each real (blue; top) and randomly selected (red; bottom) trajectory over time. **C)** The distribution of the difference in instantaneous angles and the mean angles before (gray) and after plume encounter for real (blue; top) and randomly selected (red; bottom) trajectories. Notice no difference between the before and after distribution for randomly selected trajectories (red; bottom), while the distribution after encounter for real trajectories (blue; top) becomes narrower than the distribution before (gray; top) plume encounter. **D)** The mean angle (top) over time for real (blue) and randomly selected (red) trajectories with the corresponding strength (bottom) of the resultant vector.

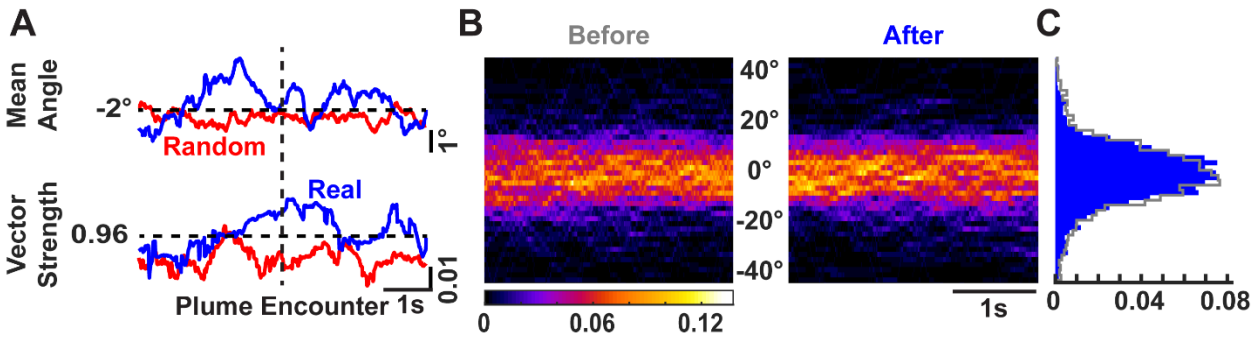

Figure 5. Mice reduce the variability of the yaw angle of head motions after plume encounter during odor-guided search. A) The mean angle (top) over time for real (blue) and randomly selected (red) trajectories with the corresponding strength of the resultant vector (bottom). Notice the increase in the strength peri-plume encounter for the real trajectories. **B)** The probability heatmap over time for left (+ve) and right (-ve) head motions before (grey) and after (blue) plume encounter. **C)** The head angle distribution before (grey) and after (blue) plume encounters.

References

Ackels T (2022) Information about space from time: how mammals navigate the odour landscape. Neuroforum 28:159–168.

Ackels T, Erskine A, Dasgupta D, Marin AC, Warner TPA, Tootoonian S, Fukunaga I, Harris JJ, Schaefer AT (2021) Fast odour dynamics are encoded in the olfactory system and guide behaviour. Nature 593:558–563.

Berens P (2009) **CircStat** : A *MATLAB* Toolbox for Circular Statistics. J Stat Soft 31.

Cardé RT, Willis MA (2008) Navigational Strategies Used by Insects to Find Distant, Wind-Borne Sources of Odor. Journal of Chemical Ecology 34:854–866.

Demir M, Kadakia N, Anderson HD, Clark DA, Emonet T (2020) Walking Drosophila navigate complex plumes using stochastic decisions biased by the timing of odor encounters. eLife 9:e57524.

Dennis EJ, Hady AE, Michaiel A, Clemens A, Tervo DRG, Voigts J, Datta SR (2021) Systems Neuroscience of Natural Behaviors in Rodents. J Neurosci 41:911–919.

Findley TM, Wyrick DG, Cramer JL, Brown MA, Holcomb B, Attey R, Yeh D, Monasevitch E, Nouboussi N, Cullen I, Songco JO, King JF, Ahmadian Y, Smear MC (2021) Sniff-synchronized, gradient-guided olfactory search by freely moving mice. eLife 10:e58523.

Karalis N, Sirota A (2022) Breathing coordinates cortico-hippocampal dynamics in mice during offline states. Nat Commun 13:467.

Lewis SM, Xu L, Rigolli N, Tariq MF, Stern M, Seminara A, Gire DH (2021) Plume dynamics structure the spatiotemporal activity of glomerular networks in the mouse olfactory bulb. Front Cell Neurosci 15.

Liao S-M, Kleinfeld D (2023) A change in behavioral state switches the pattern of motor output that underlies rhythmic head and orofacial movements. Current Biology S0960982223004566.

Liao S-M, Kleinfeld D (2022) A change in behavioral state switches the pattern of motor output that underlies rhythmic head and orofacial movements (preprint). Neuroscience.

Mafra-Neto A, Cardé RT (1998) Rate of realized interception of pheromone pulses in different wind speeds modulates almond moth orientation. Journal of Comparative Physiology A 182:563–572.

Mafra-Neto A, Cardé RT (1994) Fine-scale structure of pheromone plumes modulates upwind orientation of flying moths. Nature 369:142.

Marin AC, Schaefer AT, Ackels T (2021) Spatial information from the odour environment in mammalian olfaction. Cell Tissue Res 383:473–483.

Mathis A, Mamidanna P, Cury KM, Abe T, Murthy VN, Mathis MW, Bethge M (2018) DeepLabCut: markerless pose estimation of user-defined body parts with deep learning. Nature Neuroscience 21:1281–1289.

Michaiel AM, Abe ET, Niell CM (2020) Dynamics of gaze control during prey capture in freely moving mice. eLife 9:e57458.

Nath T, Mathis A, Chen AC, Patel A, Bethge M, Mathis MW (2019) Using DeepLabCut for 3D markerless pose estimation across species and behaviors. Nat Protoc 14:2152–2176.

Rigolli N, Reddy G, Seminara A, Vergassola M (2022) Alternation emerges as a multi-modal strategy for turbulent odor navigation. eLife 11:e76989.

Tariq MF, Lewis SM, Lowell A, Moore S, Miles JT, Perkel DJ, Gire DH (2021) Using Head-Mounted Ethanol Sensors to Monitor Olfactory Information and Determine Behavioral

Changes Associated with Ethanol-Plume Contact during Mouse Odor-Guided Navigation. eNeuro 8.

van Breugel F, Dickinson MH (2014) Plume-Tracking Behavior of Flying Drosophila Emerges from a Set of Distinct Sensory-Motor Reflexes. Current Biology 24:274–286.

Vickers N (2000) Mechanisms of animal navigation in odor plumes. The Biological Bulletin 198:203–212.

Vickers NJ, Baker TC (1994) Reiterative responses to single strands of odor promote sustained upwind flight and odor source location by moths. Proc Natl Acad Sci USA 91:5756.

Vickers NJ, Christensen TA, Baker TC, Hildebrand JG (2001) Odour-plume dynamics influence the brain's olfactory code. Nature 410:466.

Conclusions

Understanding the neural representations of the sensory cues within the environment, and how these representations guide behaviors has been one of the central pursuits in neuroscience. Olfaction is one key sensory modality that allows an animal to navigate its habitat for locations of food resources, mates and shelter as well as to avoid predation. Olfaction has also been shown to evoke intense emotions and autobiographical memories in humans (HERZ, 1998; Herz et al., 2004; Herz and Cupchik, 1995; Willander and Larsson, 2007, 2006). Odors then guide decision-making, and serve as sensory cues for a spatiotemporal map in the memory of animals.

Although much is known about the anatomical structures and activity within the neural circuits during passive presentation of olfactory information in head-fixed setups, how odor cues shape naturalistic behaviors in freely moving organisms remains poorly understood (Ackels, 2022; Marin et al., 2021). The stochastic nature of the olfactory information during the naturalistic behavior of plume tracking then serves as an excellent model for how organisms adapt their behavior to maximize their sensory information providing a tractable model to study how sensation guides motion and vice-versa.

One main difficulty of studying naturalistic plume-guided behaviors stemmed from the challenges associated with recreating the complex olfactory landscape that animals experience in the wild, and correlating the dynamic olfactory information with the behavior and neural processing. This thesis presents my endeavors, performed in collaboration with other researchers, on creating naturalistic odor stimuli in a custom-built wind tunnel to implement an odor-guided navigation task for rodents, and developing a novel method using head-mounted sensors (Tariq et al., 2021) to record the real-time olfactory information that an animal receives while engaged in this task.

Using these technologies, we show that plume encounters result in speed reduction of the freely moving mice (Tariq et al., 2021), raising the possibility that these speed reduction episodes promoted periods of active sensation of the olfactory stimulus. In Chapter 2 of this thesis, I probed this question further by combining the previously developed techniques with head-motion tracking of freely moving mice to study how/if the dynamically varying odor stimulus promotes active sensing of the olfactory information through increased amplitude and frequency of head-pitch motions. We show mice exhibit robust head motions to acquire olfactory information and these head motions are modulated upon plume contacts, suggesting head motions as an important component of a complex series of sensorimotor behavioral repertoire during naturalistic behaviors. Here, I present the limitations of the work presented in this thesis.

Limitations

One of the limitations of the work presented here is that I was not able to fully ascribe the head motions with sniffing in freely moving mice. While a number of groups have established correlations between freely moving rodents' head motions and their sniffing (Findley et al., 2021; Karalis and Sirota, 2022; Liao and Kleinfeld, 2022), I was not able to establish a direct effect of plume encounters on sniffing. For this pursuit, I designed a method using miniature pressure sensors to measure the pressure changes within the nasal cavity of mice during free behavior. This method was based on the work of Wesson et al. (2008), but their method used a long tube to carry the air pressure changes to a non-mobile pressure transducer.

Using miniature pressure sensors allowed the possibility of mounting them directly on the head of freely moving mice, reducing impedance on the motion of the animals and improving the signal-to-noise ratio by digitizing the pressure changes closer to the source. While this method

was used in reduced capacity by researchers in our lab (not published) for head-fixed setups, I was not able to implement the full design for freely moving mice. Miermon et al. (2022) independently presented on the feasibility of this principle in a recent poster presentation, so measuring nasal pressures might then be a way to achieve simultaneous head-motions and sniff tracking during naturalistic behavioral tasks in rodents.

However, sniff tracking using nasal pressures has its drawbacks. The nasal cannula can clog with mucus thus preventing pressure monitoring, and the signals can also show attrition over days which prevents this method for experiments using months-long behavioral tasks on the same animal. Another method, reported by McAfee et al. (2016) and expanded on by Findley et al. (2021), has shown a lot of promise for stability over months. This method measures the temperature changes, resulting from cooling and warming of the nasal tissue with inhalations and exhalations, for sniff monitoring. This method has some lag time and pauses between inspirations during slow breathing are not that well represented, hence, creating a challenge to precisely time neural activity (see below) with sniffing.

Another limitation is the slow response of the metal oxide sensors we used to detect the odor plumes. With the deconvolution procedure described in Tariq et al. (2021) we can increase the response time for higher frequency response, but I conjecture that these sensors can be further improved physically to optimize their performance. This optimization is possible by increased collaborations between engineers and neuroscientists. Engineering groups are focusing on using principles from animal olfaction for improved designs of olfactory robots (Fang et al., 2022; Lee et al., 2023; Milone et al., 2021; Neta et al., 2023; Persaud et al., 2013), while neuroscientists are designing rigorous experiments to study animal olfaction (Findley et al.,

2021; Gire et al., 2016; Gumaste et al., 2020; Jackson et al., 2020; Liu et al., 2020; Tariq et al., 2021) so increased collaborations between the two groups will mutually benefit both.

Another limitation is that I was not able to record neural activity during my experiments. Recent advances in neural recording, like Neuropixels (Jun et al., 2017), allow recording hundreds of neurons simultaneously at high temporal resolution. Hence, efforts to implement them in freely moving mice (Juavinett et al., 2019) will bear many fruitful results. However, the probe designs for these hardware is not compatible with the spatial aligning of the cells within olfactory brain areas. Calcium imaging using head-mountable microscopes (Ghosh et al., 2011; Zong et al., 2022) might be feasible alternatives for recording neural activity within the olfactory areas of freely moving mice. While the most recent generation of calcium sensors allow for sub-sniff recording of calcium transients (Zhang et al., 2023), head-mounted imaging hardware still suffer from low sampling rate limiting their use for the olfactory field. Gill et al. (2020) presents a method for precise stimulation of olfactory circuits. Incorporating this method in freely moving animals may open doors for many interesting experiments, but studying how freely moving animals integrate wind information with olfactory information will not be achievable with this method.

References

Ackels T (2022) Information about space from time: how mammals navigate the odour landscape. Neuroforum 28:159–168.

Fang C, Li H-Y, Li L, Su H-Y, Tang J, Bai X, Liu H (2022) Smart Electronic Nose Enabled by an All-Feature Olfactory Algorithm. Adv Intell Syst 4:2200074.

Findley TM, Wyrick DG, Cramer JL, Brown MA, Holcomb B, Attey R, Yeh D, Monasevitch E, Nouboussi N, Cullen I, Songco JO, King JF, Ahmadian Y, Smear MC (2021) Sniff-synchronized, gradient-guided olfactory search by freely moving mice. eLife 10:e58523.

Ghosh KK, Burns LD, Cocker ED, Nimmerjahn A, Ziv Y, Gamal AE, Schnitzer MJ (2011) Miniaturized integration of a fluorescence microscope. Nat Methods 8:871–878.

Gill JV, Lerman GM, Zhao H, Stetler BJ, Rinberg D, Shoham S (2020) Precise Holographic Manipulation of Olfactory Circuits Reveals Coding Features Determining Perceptual Detection. Neuron 108:382-393.e5.

Gire DH, Kapoor V, Arrighi-Allisan A, Seminara A, Murthy VN (2016) Mice Develop Efficient Strategies for Foraging and Navigation Using Complex Natural Stimuli. Curr Biol 26:1261–1273.

Gumaste A, Coronas-Samano G, Hengenius J, Axman R, Connor EG, Baker KL, Ermentrout B, Crimaldi JP, Verhagen JV (2020) A Comparison between Mouse, *In Silico* , and Robot Odor Plume Navigation Reveals Advantages of Mouse Odor Tracking. eneuro 7:ENEURO.0212-19.2019.

HERZ RS (1998) Are Odors the Best Cues to Memory? A Cross-Modal Comparison of Associative Memory Stimulia. Ann N Y Acad Sci 855:670–674.

Herz RS, Cupchik GC (1995) The Emotional Distinctiveness of Odor-evoked Memories. Chem Senses 20:517–528.

Herz RS, Eliassen J, Beland S, Souza T (2004) Neuroimaging evidence for the emotional potency of odor-evoked memory. Neuropsychologia 42:371–378.

Jackson BJ, Fatima GL, Oh S, Gire DH (2020) Many Paths to the Same Goal: Balancing Exploration and Exploitation during Probabilistic Route Planning. eneuro 7:ENEURO.0536-19.2020.

Juavinett AL, Bekheet G, Churchland AK (2019) Chronically implanted Neuropixels probes enable high-yield recordings in freely moving mice. eLife 8:e47188.

Jun JJ et al. (2017) Fully integrated silicon probes for high-density recording of neural activity. Nature 551:232–236.

Karalis N, Sirota A (2022) Breathing coordinates cortico-hippocampal dynamics in mice during offline states. Nat Commun 13:467.

Lee S, Kim M, Ahn BJ, Jang Y (2023) Odorant-responsive biological receptors and electronic noses for volatile organic compounds with aldehyde for human health and diseases: A perspective review. J Hazard Mater 455:131555.

Liao S-M, Kleinfeld D (2022) A change in behavioral state switches the pattern of motor output that underlies rhythmic head and orofacial movements (preprint). Neuroscience.

Liu A, Papale AE, Hengenius J, Patel K, Ermentrout B, Urban NN (2020) Mouse Navigation Strategies for Odor Source Localization. Front Neurosci 14.

Marin AC, Schaefer AT, Ackels T (2021) Spatial information from the odour environment in mammalian olfaction. Cell Tissue Res 383:473–483.

McAfee SS, Ogg MC, Ross JM, Liu Y, Fletcher ML, Heck DH (2016) Minimally invasive highly precise monitoring of respiratory rhythm in the mouse using an epithelial temperature probe. J Neurosci Methods 263:89–94.

Miermon C, Casali G, Chenouard N, Terral T, Dolique T, Lesburgueres E, Gambino F, Roux L (2022) High-precision monitoring of nasal pressure in freely moving mice provides state-specific respiratory features and vigilance state prediction.

Milone A, Monteduro AG, Rizzato S, Leo A, Maruccio G (2021) Gas sensing technologies -- status, trends, perspectives and novel applications.

Neta S, Ariel G, Yossi Y, Amir A, Ben MM (2023) The Locust antenna as an odor discriminator. Biosens Bioelectron 221:114919.

Persaud KC, Marco S, Gutiérrez A (Eds.) (2013) Neuromorphic olfaction, Frontiers in neuroengineering. Boca Raton, FL: CRC Press.

Tariq MF, Lewis SM, Lowell A, Moore S, Miles JT, Perkel DJ, Gire DH (2021) Using Head-Mounted Ethanol Sensors to Monitor Olfactory Information and Determine Behavioral Changes Associated with Ethanol-Plume Contact during Mouse Odor-Guided Navigation. eNeuro 8.

Wesson DW, Donahou TN, Johnson MO, Wachowiak M (2008) Sniffing Behavior of Mice during Performance in Odor-Guided Tasks. Chem Senses 33:581–596.

Willander J, Larsson M (2007) Olfaction and emotion: The case of autobiographical memory. Mem Cognit 35:1659–1663.

Willander J, Larsson M (2006) Smell your way back to childhood: Autobiographical odor memory. Psychon Bull Rev 13:240–244.

Zhang Y et al. (2023) Fast and sensitive GCaMP calcium indicators for imaging neural populations. Nature 615:884–891.

Zong W, Obenhaus HA, Skytøen ER, Eneqvist H, De Jong NL, Vale R, Jorge MR, Moser M-B, Moser EI (2022) Large-scale two-photon calcium imaging in freely moving mice. Cell 185:1240-1256.e30.